

DOE / PC94218-12

KINETICS AND MECHANISMS OF NO_x - CHAR REDUCTION

**E. M. SUUBERG (PRINCIPAL INVESTIGATOR)
W.D. LILLY (STAFF)
I. AARNA (Ph.D. STUDENT)**

**DIVISION OF ENGINEERING
BROWN UNIVERSITY
PROVIDENCE, RI 02912
TEL. (401) 863-1420**

**QUARTERLY TECHNICAL PROGRESS REPORT
1 MARCH, 1997 - 30 JUNE, 1997**

**PREPARED FOR:
U. S. DEPT. OF ENERGY
PITTSBURGH ENERGY TECHNOLOGY CENTER
P.O. BOX 10940
PITTSBURGH, PA 15236**

**DR. MILDRED PERRY
TECHNICAL PROJECT OFFICER**

"US/DOE Patent Clearance is not required prior to the publication of this document"

1. Introduction

Most industrially important carbons are produced from naturally occurring materials such as coal, oil, peat or wood by some form of thermal process. Chars are obtained from those natural materials as a residue after removal of the volatile matter. Chars (prepared from coal or other organic precursors) are non-graphitizable carbons, meaning that they cannot be transformed into graphitic carbon. Chars are comprised of elementary crystallites in parallel layers which are randomly oriented with respect to each other and are crosslinked together through weak bonds. Voids between crystallites determine the porosity of the char, and this plays an important role in char gasification behavior. Chars usually contain a pore size distribution, in which the larger macro- and mesopores play an important role in transport of reactants into the much smaller micropores, in which most gasification and combustion take place. Therefore, the effectiveness of micropores in gasification depends heavily on the numbers of meso- and macropores.

Many studies of char gasification have demonstrated that gasification rates change drastically with burn-off (or conversion), showing a maximum at intermediate levels of burn-off¹⁻¹⁰. It is believed that these changes reflect, to a large extent, changes in the internal surface area. At low levels of burn-off, pores grow due to gasification, whereas at intermediate levels of burn-off pores start to coalesce with neighboring pores causing loss of surface area which in turn causes the overall carbon mass loss rate to decrease. Some workers have also found a monotonically decreasing gasification rates with burn-off^{7,8,11} when pore coalescence dominates from the early stages of reaction.

Particle shrinkage has also been found¹² to be important in pore structure evolution during gasification. Under kinetic control conditions, particle diameter reduction seems to be a result of both perimeter fragmentation and collapse (atomic rearrangement) of the particle internal structure, which is accompanied by particle densification. Particle shrinkage is more important in gasification of highly microporous carbons (surface area

larger than $800 \text{ m}^2/\text{g}$), where gasification occurs within the microporous carbon structure. Pore collapse seems to be connected to particle shrinkage, or they may even involve the same processes.

It was realized long ago that there is strong coupling between the heterogeneous reaction rate of chars and their porous structures, and most modern models of reactivity include this feature. Hence, a good description of the initial pore structure, as well as its development, is important for modeling the reactivity of carbon in many practical situations. Much of the complexity in providing quantitative descriptions of carbon gasification behavior arises from the difficulty in describing the porous structure of char (it also reflects a poor understanding of the nature of active sites in gasification). A review of models of the evolution of porous structure during reaction has been presented several years ago¹³. Here we will not attempt to repeat the review the extensive work done on this subject, but rather highlight some of the relevant features.

The earliest gasification model to involve a porous solid is that of Petersen¹⁴, which considered a gasified solid to consist of cylindrical pores of uniform size. This model neglected the intersections of pores as the reaction surface grows. Another model developed by Szekely and Evans¹⁵ has also been commonly used. This so called “grain model” describes the porous medium as a collection of nonporous grains of different sizes and the porosity development is described by the shrinking core behavior of those grains. This model predicts the monotonically decreasing reaction rate with conversion because the reacting surface is decreasing.

A different physical picture is offered by the so-called “random pore model”, a version of which was developed by Hashimoto and Silveston¹⁶ using a population balance technique; this version contained several adjustable parameters to describe the structure. Yet another representation of the pore system was used by Simons and Finson¹⁷ and Simons¹⁸, who concluded that the pore system in chars resembles an ordinary river or tree system with small pores feeding into increasingly larger pores. They developed a semi-

empirical description of this picture in order to describe the initial pore structure and its evolution with gasification.

Perhaps the currently most widely used approach for describing reactions of porous solids is again based upon the random pore model, in a version proposed independently by Gavalas¹⁹ and Bhatia and Perlmutter²⁰. In this implementation, experimentally determined parameters of initial pore size distribution and reaction rate are used in these models to characterize the porosity development.

Drawing somewhat upon the earlier qualitative descriptions, other recent models have considered char to be comprised of two regions, a macropore "region" and a micropore "region". In this case there should be different models to describe the porosity in different regions. Sandmann and Zygourakis²¹ developed a discrete model which allows modeling the pore development in char with a multimodal pore size distribution, in the presence and absence of pore diffusion limitations and in the presence of particle fragmentation. Bhatia²² proposed a model for coal to be comprised of microporous grains, with the random pore model holding for the micropores in the grains. Ballal and Zygourakis²³ developed novel random pore models for predicting changes in porosity of both unimodal and bimodal pore size chars, in which the model parameters are directly related to the structural properties of "raw" char. Another model that separately described macroporosity and microporosity was recently proposed by Kantorovich and Bar-Ziv^{24,25}. In this work a new picture for pore structure evolution were proposed. Whereas usually uniform pore diameter increase with reaction is assumed (i.e. the surface concentration of active sites is constant during reaction), in this study the changes in concentration of active sites were modeled as involving coalescence of the microcrystals. Using this model, in which changes in dimensions and coalescence of graphitic "microrods" took place, the authors were able to explain the shrinkage phenomenon and the evolution of internal surface area of highly porous carbons in the intrinsic reaction regime.

These modeling approaches have generally been developed for use only in the purely kinetically controlled regime, and only some workers have extended their models into the pore diffusion limited regime^{21,26-28}. It is of course easily imagined that the physical picture is greatly complicated when transport limitations in the pores are present as the pores are themselves enlarging.

Most of the earlier described models assume the absence of new pore generation and none of the above models accounts for the opening of initially closed pores. The latter is important in many "raw" or ungasified chars. All these models also assume that all measurable surface area (porosity) in chars is accessible to reactant in the intrinsic reaction rate control regime. This might not be true in cases in which very narrow micropore sizes require activated diffusion to be the main transport process. Gasification rates could become limited by micropore diffusion in some narrow fraction of these pores even when there is no significant concentration gradient within the particle.

Another restriction of the usual models is that most are developed to predict porosities and the evolution of porosities with burn-off in the absence of ash. These models usually assume no variation with gasification in the number of active sites per unit of surface area. This may be quite restrictive, especially when even a small amount of catalyst is present, or when thermal annealing might be taking place at high temperatures. Issues related to changes in catalyst dispersion or coating of the carbon surface are particularly difficult to incorporate into the models, but may be important in certain practical cases. Additionally, many chars contain very ordered regions which largely define their micropore structure. In this case, the assumption of a uniform distribution of active sites may be questionable, and the active site densities may actually vary with pore size. The same issue has been raised with respect to catalyst distribution⁹. Another problem with existing models is that at high levels of burn-off (above 80%) particles may disintegrate, which requires an abrupt change in the nature of most model calculations.

Objectives of the present study

Total porosity includes pores ranging from 1 Å to 10 μm (ranging over 5 orders of magnitude), and there remains a key question as to whether all these pores are used during gasification, and how they are used. The possibilities of roles for activated diffusion limitations, of non-uniform active site density have been raised together with a number of other concerns. Thus we are interested in providing more experimental insights into how effectively porosity, in different size ranges may be used during gasification. There are different definitions of effectiveness of use. For example, there is no doubt that the role of the largest pores is limited, in one sense, because of their very small contribution to the reactive surface area. However they play a key role in feeding the interior of the particle. It is thus important to track, during reaction, the changes in all size ranges of pores, and not simply track surface area, in order to understand how all pores are being used. In this work, we are also very interested in determining the smallest pores which can be used in gasification, since this is critical to gaining a better understanding of how to model the gasification reaction and its surface area dependence.

In this report we present results on the nature of porosity development during gasification of two carbons under certain conditions. The current report compares porosity development in Wyodak coal char and a tire-derived char gasified in three different oxidizing gases (nitric oxide, oxygen and carbon dioxide). To help characterize the development of the pores, standard gas adsorption techniques have been used on quenched char samples. From the isotherms, several distinct pieces of information may be obtained. The first is an estimate of micropore volume, the second is an estimate of pore size distribution and the third is total surface area. The characterization of the pore size distribution is critical in many respects, but no definitive characterization method suitable for all porous materials has been developed. We rely on standard methods, but will point out where these may be wanting. Finally, we close with suggestions for improvements to current pore transport models.

2. Experimental

2.1 Sample Preparation and characterization

Wyodak coal samples were obtained from the Argonne Premium Coal Sample Bank²⁹. Wyodak is a subbituminous coal and contains 6.3% ash as received. Table 1 shows the proximate and ultimate analysis of the Wyodak coal. Wyodak coal samples (particle size <250 μm) were pyrolysed in a tube furnace at 1273 K for two hours, in a flow of high purity helium. The char produced is microporous, with some mesoporosity as well, and exhibits initial N₂, Ar and CO₂ BET surface areas of 127, 47 and 272 m²/g, respectively. Such a trend is well known and illustrates the difficulty in selecting the "correct" gas for pore analysis.

Tire char was selected as a second model material in this study because of its highly mesoporous structure. Samples were prepared from used tires by pyrolysis at 973 K in nitrogen for 5 minutes and were further pyrolysed at 1173 K for one hour in helium before gasification. These chars are called "raw" tire chars.

Adsorption isotherms and specific surface areas were determined in an automated volumetric gas adsorption apparatus (Autosorb 1, Quantachrome Co.). By performing a dead volume correction with helium, the instrument calculates the amount sorbed using a differential pressure technique. Adsorption of N₂, Ar and CO₂ were performed at 77 K, 77 K and 195 K, respectively. Before the experiments, the samples were all outgassed at 672 K for at least 8 h in vacuum at about 10⁻² Torr.

Long equilibration times were needed for chars with low levels of burn-off (usually less than 5%) during nitrogen and argon adsorption measurements at low relative pressures. This resulted in low pressure hysteresis loops. The long equilibration times indicate the presence of a large number of micropores whose diameters are comparable to the diameter of adsorbate molecule. Activated diffusion is a predominant mode of mass

transfer in small micropores, resulting in slow diffusion rates. This is the reason for the sensitivity to choice of probe molecules. Surface areas, from N₂ and Ar adsorption at 77 K and from CO₂ adsorption at 195 K, were calculated using the BET equation. The use of higher temperature for CO₂ measurements is thought to help overcome some activated diffusion energy barriers - hence higher apparent areas with CO₂ for the raw chars.

Determination of pore size distribution from N₂, Ar and CO₂ adsorption isotherms were performed using Barrett, Joyner and Halenda³⁰ theory. It is understood that this might be not a very good choice for micropores, because this theory is based upon the Kelvin equation, which is not valid in narrow micropores. The use of more generally accepted DFT method³¹ was also not justified, because this method was created for analysis of very microporous materials. It does not work well when mesopores are present. Moreover, this method was developed only for characterization of nitrogen adsorption isotherms.

In this study three adsorptives (N₂, Ar and CO₂) were used to characterize the porosity, in order to get more reliable information on the chars. Many adsorbates have been proposed to characterize the porous structure of solids³², all of them should meet a number of minimum criteria: chemical inertness, relatively large saturation pressure and a molecular shape close to spherical. Nitrogen is the most widely used adsorbate and it approximates these conditions, but it has a problem of presenting a permanent quadrupole moment. The second adsorbate, argon, has similar physical properties to nitrogen. The adsorption temperature used (77 K) was however below the triple point of argon (88.8 K), and therefore there is doubt concerning the appropriate reference state of argon. This leads to an uncertainties in the estimates for the cross sectional area of argon. As implied above, when nitrogen or argon is used to characterize microporous materials, either may present an additional problem because of the low temperature of measurements (77 K), and the resulting concern about activated diffusion effects. Thus an increase in adsorption

temperature can lead to an increase of the amount of nitrogen adsorbed contrary to what is predicted on thermodynamic grounds.

It has been proposed by some authors^{33,34} that use of CO₂ as an adsorbate is preferred to that of nitrogen because of the higher temperatures of adsorption which can be used (195 K in our case). There is still an uncertainty about the state of the CO₂ adsorbed in micropores and therefore about the cross sectional area of the CO₂ molecule. Carbon dioxide has a high quadrupole moment, like nitrogen, which means that its adsorption isotherm is very sensitive to the presence of polar groups or ions in the surface of adsorbent³². There are also other issues associated with use of CO₂, as will be noted below. Important physical parameters of different adsorbents used in surface area and pore size distribution calculations are given in Table 2.

2.2 Apparatus

The char reactivity measurements in different oxidizing atmospheres were performed in an Online Instruments TG-plus thermogravimetric analyzer. The reactions were performed in a flow of helium/reactant gas (O₂, NO or CO₂) mixture, with a purge gas flow rate about 220 cm³/min. The temperature and sample mass were recorded as a function of time. Products formed during the experiments can be analyzed using the attached FTIR spectrometer, fitted with a multipass gas cell. Samples of 30-50 mg were dispersed on a circular platinum pan with a large flat surface and raised sides, resulting in a thin particle beds. The sample bucket was located in the heated zone of the TGA furnace, and a K-type thermocouple was placed about 5 mm from the sample. Temperatures between 773-973 K were used for gasification with NO and CO₂, whereas temperatures between 573-748 K were used for O₂ gasification. The partial pressures of oxidizing gases were 0.82, 2.02 and 4.80 kPa for NO, O₂ and CO₂, respectively.

2.3 Experimental procedure

The experimental protocol employed during the reactivity measurements consisted of four steps:

- (1) The char samples were outgassed at 1173 K for 30 min to clean the surface of adsorbed moisture and oxygen.
- (2) Samples were activated in the oxidant gas (NO, O₂ or CO₂) up to the desired level of burn-off (up to 5% in reactivity measurements).
- (3) Samples were outgassed again at 1173 K for 1 hour to remove the surface complexes.
- (4) Sample reactivities were determined. These were consecutively measured at different temperatures, using the same sample, by increasing temperature step by step. Therefore, the reactivities at different temperatures were measured at different levels of burn-off, but the change in burn-off during the reactivity measurement was relatively small (about 5%) and did not introduce a significant uncertainty in rates, because surface area does not vary much with burn-off in this range.

For the preparation of samples with different levels of burn-off, only the first two steps were employed. In this way char samples at different levels of burn-off were prepared in different oxidizing gas atmospheres. The adsorption characteristics were determined for all of these samples.

The carbon burn-off during gasification has been defined as:

$$X = \frac{m_0 - m}{m_0}$$

where m_0 is the initial mass of char on dry, oxygen complex free and ash free basis, and m is a sample mass at a given moment, on an ash free basis. The gasification rate has been defined on different bases: on initial mass basis $\frac{1}{m_0} \frac{dm}{dt}$, on remaining mass basis $\frac{1}{m} \frac{dm}{dt}$, on surface area basis $\frac{1}{A} \frac{dm}{dt}$, and on total pore volume basis $\frac{1}{V} \frac{dm}{dt}$. The relevant methods will be cited as the results are presented.

3. Results and discussion

3.1 Chemical kinetic control regime (Zone I)

Dynamic changes in char reactivity and pore structure during gasification have been studied to a limited extent. The need to study the porosity development with burn-off is important in the modeling of combustion and gasification. The most important surface properties of chars are the internal surface area and pore size distribution, which determine gas diffusion and reaction rates within the particle. The characterization of porosity in chars is not an easy task since there is no single technique that can provide information about the full range of porosity. The most widely used method for characterizing porous carbons is the adsorption of gases. In this section, the emphasis is on the changes in porosity during gasification in the chemical control regime.

3.1.1 Reactivity of Wyodak coal char

It is well known that a porous solid-gas reaction can be characterized by three reaction regimes, namely kinetic control (Zone I), pore diffusion control (Zone II) and film diffusion control (Zone III). The temperature dependencies of gasification rates in NO, O₂ and CO₂ of Wyodak coal chars are presented in Figure 1. Our NO and CO₂ gasification data show that in the kinetic control regime two subregimes can be distinguished two subregimes, where higher activation energies are found in the high temperature regime. Those two temperature regimes are caused by different controlling reaction mechanisms. The two temperature regime behavior is well established in NO gasification³⁵, but in spite of the long history of CO₂ gasification research, we know of no other reports of two temperature regime behavior in CO₂ gasification. The third gasification reaction, namely oxygen gasification, is governed by a single activation energy at the experimental conditions studied. Figure 1 shows that the gasification reactivities decrease in order O₂ > NO > CO₂, when expressed on surface area normalized bases.

Surprisingly, there is evidence in Figure 1 of zone II behavior in NO gasification. This zone is generally observed in the presence of pore diffusion limitations. It is interesting to note its occurrence in NO despite the low reactivities involved (compared to oxygen). Note that Figure 1 shows apparent rate constants, assuming first order with respect to reactant gas. Since the partial pressure of oxygen was a factor of 2.5 times that of NO, the actual rates in oxygen achieved higher values in that gas, but still showed no Zone II behavior. This is one of the first clear indications of pore diffusion limitations in NO gasification. The activation energy in zone II is about one-half of the activation energy of the high temperature regime, as a random pore model would require, lending support to this type of model. The existence of zone II in NO gasification gives us an unique opportunity to study the porosity development at those conditions, which will be discussed in section 3.3.

3.1.2 Description of adsorption isotherms on Wyodak coal char

Representative nitrogen, argon and carbon dioxide adsorption and desorption isotherms on Wyodak coal char are given in Figure 2. This particular char was gasified in NO at 911 K to 34.8% burn-off. The nitrogen isotherms obtained for Wyodak coal char are a combination of types I and II. The nitrogen isotherm shape indicates that in addition to micropores there exists a well developed mesoporosity, which gives rise to a significant slope of the isotherm plateau. The isotherm has an hysteresis loop of the H3 type according to the IUPAC classification³⁶, corresponding to adsorbents having slit-shaped pores.

The shape of the argon isotherm is consistent with type I, which is indicative of microporosity. The isotherm of argon has a type H4 hysteresis loop again associated with narrow slit-like pores. The time needed to reach equilibrium was long in both nitrogen and argon adsorption and all points were taken in a similar manner at some quasi-equilibrium state. Long equilibration times are caused by constrictions with dimensions comparable to adsorbate molecule. Despite the similarities of physical properties of nitrogen and argon,

their adsorption isotherms are different at high relative pressures ($P/P_0 > 0.2$). The hysteresis loop of argon isotherm also closes at lower relative pressure ($P/P_0 \approx 0.3$). This seems to indicate the differences in capillary condensation mechanisms, whereas the micropore filling is similar (note that the pore volumes at low P/P_0 are very similar with both these gases).

The carbon dioxide isotherm on Wyodak coal char is type I with low pressure hysteresis. This may be expected with CO_2 in a microporous sample. The observed low pressure hysteresis loop in this isotherm could arise from insufficient adsorption times. Since the adsorption temperature used for CO_2 was higher than 77 K, the apparent equilibration times were much shorter, but still perhaps not enough to reach true equilibrium. This explanation might be troublesome to those used to thinking that CO_2 is not subject to the same activated diffusion barrier as N_2 . It should however be recalled that there is a continuum of micropore sizes, and that CO_2 might indeed be able to penetrate where N_2 cannot especially in very small micropores. The smaller the gap that needs to be penetrated, the longer the equilibration time. It is fair to note that the amount of such porosity is very small, since the hysteresis loop is not at all large. Naturally, the much lower uptake of CO_2 than N_2 or Ar at low values of P/P_0 must have a different explanation, not based upon ability to penetrate. It is well established that CO_2 is not adequate for probing microporosity, in certain cases³⁷. The reason presumably has to do with its inability to condense in some range of microporosity. It has been proposed³⁷ that N_2 can fill both wider micropores and mesopores, whereas CO_2 can fill only narrow micropores or be adsorbed in a surface coverage mechanism. This indicates that CO_2 and N_2 detect different types of porosities, which explains the different types of isotherms obtained by the different adsorbate gases.

3.1.3 Surface area and pore volume development

It was realized a long time ago that there is a strong coupling between the heterogeneous reaction and the porous structure of char. A heterogeneous reaction, such as a gasification reaction, takes place on active surface sites. The numbers of these sites are somehow related to surface area with the most usual assumption being a direct proportionality. Therefore, the development of surface area is a very important aspect of gasification. During gasification, surface area increases up to a point at which the rate of formation of new area is offset by the rate of destruction of the old area. Surface area usually passes through a maximum at some intermediate burn-off. This behavior has been found during CO₂ gasification for many carbonaceous materials such as coal chars^{1,6,7,9}, polymer carbon³⁸, anthracite³⁹, peat⁴⁰. The same general behavior has been reported during steam gasification for bituminous coal char and anthracite⁴¹ coal chars and coconut shell char⁴². Even single particle experiments with Spherocarb in an electrodynamic chamber showed that surface area passes through a maximum at around 15% burn-off⁴³.

Here, we will compare how different oxidizing gases develop porosities in the chemical reaction limited regime (Zone I). Surface areas were calculated from N₂, Ar and CO₂ adsorption isotherms using the BET theory and are presented in Figures 3, 5 and 6, respectively. From N₂ and CO₂ isotherm data the total pore volumes were also calculated at relative pressures of 0.995 and 0.90, and are presented in Figures 4 and 7, respectively.

Many phenomena determine the evolution of the pore structure: pore opening, pore growth, "coalescence" of neighboring pores, diffusion limitations, particle shrinkage, particle fragmentation, etc. According to Rodríguez-Reinoso⁴⁴ there are three mechanisms available to explain porosity development: i) pore deepening, widening or enlargement, ii) the drilling of new pores and iii) the opening of closed pores. According to Marsh *et al.*³⁸ porosity development can usually be described in terms of pore deepening and opening of closed pores only. Verma and Walker⁴⁵ showed that oxygen gasification of carbon molecular sieves at low temperatures always increases the mean diameter of micropores.

Thus the literature evidence suggests that the drilling of micropores during gasification is improbable, and gasification likely proceeds by removal of edge atoms (pore deepening) and "uncovering" of pore entries.

Our nitrogen BET surface area evolution curves in Figure 3 show that during the initial stages of gasification, a very steep increase in surface area occurs. The total porosity of the carbon may not always be accessible to reactant at low levels of burn-off because it is blocked by the carbon deposited during pyrolysis, or because some of the carbon crystallites formed closed structures. New surfaces become available after only a small extent of gasification (after about 1-2% burn-off). Therefore, it seems probable that opening of closed pores is the main process during the first few percent of burn-off, because it is otherwise unclear why there is so much development of porosity with so little carbon removal. Further development of porosity is most likely through pore drilling and pore enlargement, with the latter the most probable. Surface area passes through a maximum at around 35-50% burn-off in this case. At these intermediate levels of burn-off, pores start to coalesce with neighboring pores which causes the surface area to decrease. Some degree of particle shrinkage might also occur, which could close off micropores. The general shape of the surface area evolution curves in different atmospheres is similar, but quantitatively different surface areas are developed. Oxygen gasification creates the highest surface areas in Wyodak coal char, and these areas are only about 40 m²/g higher than obtained in NO gasification. Surprisingly, CO₂ gasification does not create high surface areas at intermediate conversions (between 10 and 60%); CO₂ is one of the most often used activation gases in production of high surface area activated carbons: The reasons for the quantitative differences in surface area evolution will be discussed in section 3.2.

Since most of the surface area is contained in the micropore region the total surface area shows the development of micropores. Pore volume development however shows the evolution of all pores. In Figure 4 the total pore volume development during gasification in different atmospheres, calculated from the N₂ adsorption isotherm is presented. The

general trend is similar to surface area with some exceptions at higher levels of burn-off. In the kinetically controlled regime there is a huge increase (almost 3-fold increase) in pore volume during the first few percent of burn-off, which again strongly suggests that there is an opening of closed porosity involved. After the first few percent there is an almost linear increase in pore volume due to pore enlargement. As expected, pore volume passes through a maximum at higher burn-off levels (over 60%) than does surface area, because the former takes into account the contributions from larger pores.

Argon BET surface area evolution curves are very similar in shape to N₂ curves (see Figure 5), the only difference is that quantitatively Ar surface areas average 100 to 150 m²/g lower. The quantitative differences may either come from an incorrect assumption regarding Ar cross sectional area (14.2 Å) or from differences in accounting for mesopore areas. The difference in the slope of the isotherms favors the latter explanation

The CO₂ BET surface area evolution curves, shown in Figure 6, give a completely different picture. We have to keep in mind that CO₂ characterizes primarily the narrowest micropores³⁷. Initially there is a small increase in surface area due to opening of closed porosity, but it is not nearly as large as observed with N₂ or with Ar. The initial increase is again followed by decrease in surface area, which reflects the destruction of micropore surface area. This involves destruction of "old" area due to pore enlargement.

In most instances, the maximum area occurs at levels of burn-off lower than what was observed with nitrogen or argon. Comparison of the areas obtained with the three adsorption probes at 20% and 60% burn-off are shown in Tables 3 and 4, respectively. Nitrogen generally provides the highest values and argon the lowest, with CO₂ in between with one notable exception for NO char, Zone II. This seems to support the notion that N₂ is most effective at probing the micropores (which contribute most area). On the other hand, the fact that the surface area begins to decline sooner for CO₂ is very evident when comparing Figures 3 and 5. In fact, the surface area change between 20 and 60% burn-off is judged to be quite modest, when examined with N₂ and Ar, and very significant when

examined by CO₂. The suggestion is that the smallest micropores, those primarily responsible for CO₂ area are disappearing due to pore enlargement. The CO₂ results are most sensitive this loss. Since these smallest micropores are filled in a manner not entirely consistent with BET theory, the implication is that the true reactive surface in non-molecular sieving pores is not well tracked by CO₂.

Quantitatively the differences between gasification agents as revealed by CO₂ isotherms are small; NO and O₂ develop slightly higher surface areas, and even in the pore diffusion limited reaction with NO the CO₂ surface area evolution is similar. There is clearly loss with burn-off of small microporosity, as revealed by CO₂, even under Zone II conditions in NO. This cannot necessarily be used to infer that reaction is occurring in these micropores, however. The percentage loss of area is modest, so it is possible that some micropores are reacting and others not. The loss might also be attributable to coalescence processes.

The CO₂ pore volume development curves do not drastically differ in shape from the surface area curves, see Figure 7. This again suggest that CO₂ cannot condense in mesopores. The surface area and pore volume revealed by CO₂ are largely attributable to condensation in small micropores. It is, however, notable that the Zone II NO char shows the slowest loss of volume in the small micropores - again consistent with lack of enlargement in this range of porosity. Quantitatively NO and O₂ gasification grow pore volumes more effectively than does CO₂ gasification. Interestingly, there is almost no difference in pore volume evolutions between CO₂ gasification in Zone I and NO gasification in Zone II. This suggests a possibly limited utilization by CO₂ of micropores even in the kinetically controlled regime.

3.1.4 Changes in adsorption isotherms during gasification

Figure 8 shows the adsorption isotherms of nitrogen on Wyodak coal char at different levels of burn-off in NO at 911 K. It was observed that the equilibration times

during N₂ adsorption at 77 K were long for samples with low levels of burn-off (< 10%). These results indicate that the pore dimensions of some pores are similar to those of the N₂ molecule, causing the adsorption to take a long time, presumably because of activated diffusion. At higher levels of burn-off this restricted diffusion phenomenon diminished. The evolution of the N₂ isotherms with burn-off qualitatively indicates that there is a slight widening of the micropores, because there is an opening of the knee of the isotherm. An increase in the mesoporosity is observed from the increase in slope of the isotherm at intermediate relative pressures. A formation of macropores during gasification can be concluded from the increase of slope of the isotherm at high relative pressures.

The adsorption isotherms of argon on Wyodak coal char at different levels of burn-off in NO at 911 K are presented in Figure 9. When the adsorption isotherms of Ar at 77 K were determined, it was found that the adsorption was even slower than in nitrogen. Activated diffusion of Ar is expected to be slower, because the effective molecular dimension of Ar is larger than that of N₂ (see Table 2). The shape of the Ar isotherm is of type I, where at low levels of burn-off a very steep initial branch is followed by an almost horizontal plateau. Once the micropores have been filled with the adsorbate the amount adsorbed remains almost constant for higher relative pressures. As the burn-off increases there is an opening of the knee of the isotherm with a more gradual approach to the plateau, which becomes less well defined. Increasing activation then appears to result in an increase of the microporosity along with creation of meso and macroporosity, though care must be exercised in advancing the latter conclusion.

Argon is apparently unable to undergo Kelvin-type condensation in meso and macropores, unlike N₂ which clearly does. Thus it reveals clearly the same increase in microporosity with burn-off as does N₂ (revealed by uptake near $P/P_0 = 0$), but cannot reveal the increase in the meso- and macropores as does N₂. It is unclear why at very high burn-offs the Ar begins to show a process like mesopore filling. It is unlikely that this is

really what is occurring. Rather, there may be a shifting of the micropore population, due to enlargement, which begins to abruptly manifest itself.

Figure 10 shows the CO₂ adsorption isotherms for Wyodak coal char with increasing degree of burn-off. The basic character of these isotherms is type I, but the shape changes slightly with burn-off. The main difference between CO₂ isotherms is in the micropore volumes, which increases with burn-off. The knee does not open during the activation, indicating that there is no pore widening except again at the highest burn-offs. It is suspected that the slope of the isotherms at intermediate values of P/P₀ is somewhat like the behavior seen at high burn-offs in Ar. It is unlikely that it is revealing mesoporous character as does the N₂. Rather, there is a pressure dependence of filling the micropores. This view receives support from the fact that the shift in the slope of the isotherms at intermediate P/P₀ abruptly increases for CO₂ just as it did for Ar, at 48.3% and 67.9% burn-off.

When the adsorption of N₂ and Ar at 77 K is compared with adsorption of CO₂ at 195 K at different levels of burn-off in NO, somewhat different behaviors can be found, see Figure 11. At low relative pressures (P/P₀ < 0.1) N₂ and Ar adsorption isotherms are very similar at all levels of burn-off, the largest difference can be found at zero percent conversion. At higher relative pressures important differences arise, again because Ar condenses less readily in mesopores. The CO₂ isotherms differ from N₂ and Ar isotherms at almost all levels of burn-off. Generally, three different regions can be observed, where:

- i) CO₂ pore volume is larger than N₂ and Ar pore volume, burn-off between 0 and 3.8%;
- ii) CO₂ pore volume is comparable to N₂ and Ar pore volume, burn-off is equal to 3.8%;
- and iii) CO₂ pore volume is smaller than N₂ and Ar pore volume, at burn-off larger than 3.8%.

The same behavior has been seen by Rodríguez-Reinoso and Linares-Solano³⁷, where they explained this phenomena with the increase in micropore diameter. At low levels of burn-off CO₂ can diffuse more readily than N₂ and Ar, because of its smaller molecular dimension and higher adsorption temperature. As burn-off increases, the

differences between CO₂ and N₂ surface areas decrease, indicating a gradual widening of the micropores, which become more accessible to both adsorbates. At high levels of burn-off the mesoporosity has increased at the expense of micropores and CO₂ cannot condense in mesopores, therefore giving lower pore volumes.

Different adsorbates thus offer quite different pictures about the porosity and its development during gasification.

3.1.5 Changes in pore size distributions during gasification

Pore size distributions (PSD) for Wyodak coal char determined at different levels of burn-off in NO, O₂ and CO₂ are shown in Figures 12, 13 and 14, respectively. The PSD's are calculated from the adsorption branch of the N₂ isotherm. By comparing Figures 12, 13 and 14 one can see that differences in the PSD's of Wyodak coal char from different oxidizing gases are minimal, allowing for a general discussion of the changes in PSD's during gasification.

The PSD's of Wyodak coal char is bimodal, with peaks in micro- and mesopores, here only the meso- and macropore regions are shown since the micropores were earlier discussed. The interesting feature of all the PSD's is that after only one percent burn-off the pore volume of mesopores (here pores between 10 and 100 Å) has increased almost three times. This again indicates the importance of a pore opening step. Of course, here one is at the mercy of the BJH PSD model, which suggests that the slope observed in the 0.9% burn-off isotherm in Figure 8 is entirely attributable to a Kelvin equation type of pore filling. On the other hand, Figure 2 has suggested that such a model may be unrealistic below $P/P_0 = 0.45$, at which the adsorption/desorption hysteresis loop closes. At this relative pressure, the BJH method assigns pores to roughly 30 Å, which means that pores that actually are governed by micropore behavior are being misassigned to mesopore size ranges. There can, however, be little doubt about the technique above about 30 Å.

After 1% conversion the pore volume in apparent mesopores increases very slowly and reaches its maximum peak height at about 50% conversion. The slow increase seems to be due to a pore creation or opening process in NO and O₂, but a pore enlargement in CO₂ gasification. Note that the peak size in the 10-100 Å range does not shift with burn-off in NO and O₂, but does trend to move towards larger pores in CO₂ gasification. Again there is some question as to the applicability of BJH method in the 10 to 30 Å range. Still, the similarity of behavior in NO and O₂ stands in contrast to that in CO₂. Here, it is observed that there exists a slight difference in pore development in different oxidizing gases, in the macropore region. In NO and CO₂ the pore volume in macropores seems to start to increase earlier than in O₂. Such a difference would not show up in a comparison of surface areas, since macropores contribute relatively little to the total surface area in this case. The different penetration depths of different molecules might play significant role here as will be discussed in section 3.2.

3.1.6 Reactivity vs. burn-off curves

A number of studies of char gasification have demonstrated that gasification reactivities change drastically with burn-off, showing a maximum at an intermediate levels of burn-off¹⁻¹⁰. It is believed that these changes reflect to a large extent changes in the internal surface area in the intrinsic reaction rate regime. At low levels of burn-off, pores grow due to gasification and also due to opening of closed pores, while at intermediate levels of burn-off pores start to coalesce with neighboring pores which causes the rate to decrease.

The reactivity vs. burn-off curves for NO, O₂ and CO₂ gasification of Wyodak coal char are given in Figure 15. Here the reactivity is expressed as, $\frac{1}{m_0} \frac{dm}{dt}$, where m_0 is the original mass of sample and m is its mass at time t . The O₂ and CO₂ gasification curves look similar, in that there is a rapid increase in reactivity during a first few percent of conversion, followed by a plateau between 5 and 20% burn-off and a gradual decrease after

20% burn-off. In NO gasification the initial increase in reaction rate is more gradual and lasts to 15% burn-off. This is followed by an almost constant reactivity thereafter.

Naturally a better way to express the rate for a disappearing solid might be as: $\frac{1}{m} \frac{dm}{dt}$, where the rate is normalized by remaining mass rather than by initial mass. This is equivalent to expressing the rate as $\frac{d(\ln m)}{dt}$, a plot of which is shown as Figure 16. This is seen to shift the curves, and change their form. Note that where $\frac{1}{m_0} \frac{dm}{dt}$ was relatively constant with burn-off in NO, now it is seen that the reactivity increases in terms of $\frac{1}{m} \frac{dm}{dt}$. In contrast, a reactivity which decreased linearly with burn-off (as in O₂ and CO₂) now is seen to increase with burn-off.

In a study by Ballal and Zygourakis^{8,46} it was shown that gasification of Illinois #6 char in CO₂ and O₂ produced a different reactivity vs. burn-off curves. Reactivity defined as $\frac{1}{m} \frac{dm}{dt}$ decreased linearly with conversion for CO₂ gasification, whereas a maximum in the rate versus conversion curve was observed for O₂. These differences were attributed to different fractions of internal surface area used during reaction in these gases. A gasification of bituminous coal char in steam and CO₂⁴⁷ also exhibited very different behaviors. Reactivity decreased linearly with conversion for steam gasification, whereas a maximum in the rate versus conversion curve was observed for CO₂. Those results clearly indicated that reactivity vs. burn-off curves obtained for a specific pair of char and reactant cannot be generalized to other gasification reactions of the same char. Our results also seem to support the view that there are some differences in reactivity vs. burn-off behavior among different reacting gases, but that these can be somewhat reduced by representing the data as $1/m(dm/dt)$. Dramatic differences in surface area development have also been found. The NO gasification results at different temperatures seem to indicate that temperature effects are not negligible either.

Several studies have demonstrated that char reactivities are not well correlated with measured N₂ or CO₂ BET surface areas^{1,48}. Our O₂ and CO₂ results seem to indicate that

the reactivity does not follow exactly the N₂ BET surface area evolution. Figures 17-19 show the data of Figures 3 and 16, 5 and 16, and 6 and 16 plotted to show variation of reactivity with BET surface areas obtained with N₂, Ar and CO₂, respectively. It has been suggested that at very low burn-off levels reactivity per N₂ BET surface is very high because nitrogen adsorption underestimates the surface area⁷, therefore CO₂ surface area might be more appropriate. This is why the results of Figures 17 through 19 are shown normalized with respect to the rate at 1% burn-off, to avoid distorting the curves due to pore opening at low burn-offs. If the rate simply tracks the further development of surface area, as indicated by the particular adsorbate gas, then the normalized reactivity curves should be flat at a value of unity.

It appears that the O₂ and CO₂ gasification reactivity curves follow closely the N₂ and Ar BET surface area curves over a range of burn-off to 70%. However, the NO gasification curve does not match closely any of the BET surface area development curves, and its normalized reactivity is seen to deviate markedly from unity on Figures 17 through 19. This supports the view that O₂ and CO₂ reactivities follow the surface area development, and raises the point that NO gasification cannot follow “normal” surface area development patterns, even under nominal Zone I conditions.

It appears that early (low burn-off) gasification reactivities in oxygen and carbon dioxide can be normalized with micropore surface area as revealed by N₂ or Ar, since both increase strongly with burn-off. Thereafter, the establishment of a constant rate per unit of remaining mass in CO₂ and O₂ gasification (for burn-offs between 20 and 60%) is reflected in the relative constancy of surface areas measured using N₂ or Ar as opposed to CO₂ which suggested a continuous decrease. Thus it appears that intrinsic rates in O₂ and CO₂ may be best correlated using N₂ surface areas, except for the very lowest levels of burn-off (<1%).

If the nitrogen surface area results of Figure 17 are considered by themselves, it appears that there is a significant period of constant reactivity per unit of surface towards

NO (from about 5 to 35% burn-off), and that the large changes in surface area that occur during this period are indeed reasonably tracked. The problem in this period is that the normalized value of reactivity is about 1.5, rather than unity. This suggests that the initial normalization was somehow not correct. This could reflect the fact that the microporosity at 1% burn-off could not be fully utilized, such that the reaction was actually taking place on a smaller area. Using the correct area would have raised the true value of $[(1/A) (dm/dt)]$ and that would have allowed the normalization to unity. This alone is not proof of this hypothesis, but it is consistent with many other results presented below. The implication would be that NO is unable to penetrate all micropores, until they are more completely opened. This would be consistent with the hypothesis that NO exists as a dimer species (hence, a larger species) within the pores of the char⁴⁴. Thus, the NO reactivity per unit surface area apparently increases because at 1% burn-off the small micropores are counted as reactive surface, whereas they are not. This, however, cannot yet explain the further increase in normalized NO reactivity at higher burn-offs (above 35%), unless the same explanation is applied again to imply that even at between 5 and 35% burn-off the micropores are not fully accessible. In fact, there is evidence to support this.

It was earlier noted that the isotherms of all three probe species showed distinctly different trends above 35% burn-off, as compared to below. The nitrogen isotherms (Figure 8) suggested a decrease in the smallest micropores above 35% burn-off, with an increase in larger pores and total porosity. The argon isotherms (Figure 9) also showed a loss of small microporosity, and a development of a slope in the plateau region of the isotherm, which was attributed to development of larger micropores. The carbon dioxide isotherms of Figure 10 showed a distinct loss of small micropores. Thus where the normalized reactivity appears to increase sharply, there is clearly a decrease in smaller micropores, and an increase in larger. Again, the suggestion is that the normalization was based upon an incorrectly high estimate of total reactive surface, and the reason that the

reactivity per unit of measured area increases at high burn-offs is that a greater fraction of the area becomes useful.

If only the larger pores were responsible for determining the reactive surface area, then a normalization of reactivity based upon pore volume, as opposed to pore surface area, might be expected to be better. Such an analysis is presented in Figure 20, based on the nitrogen pore volumes. The fit is worse for oxygen and carbon dioxide gasification than with the total surface area, but this is not surprising. The fit is slightly better for NO gasification, suggesting that this approach may be too simplistic, but in the right direction.

Instead of an explanation based upon limited access of NO into micropores, there is the possibility that the active sites for this reaction are different than for the other reactions, and are also differently distributed in various pore size ranges. The active sites could of course be catalytic sites or crystallite edges. The hysteresis loop of N₂ and Ar isotherms suggested that the mesopores in Wyodak coal char are slit shaped, representing regions between basal planes (graphitic regions). Graphites have been shown to have lower reactivities towards oxygen than disordered carbons⁴⁸. If the NO gasification reactivities of graphitic carbons are higher towards NO than towards the other gases (as has been suggested⁴⁹), and if the fraction of micropore surface which is graphitic is higher than the fraction of surface which is graphitic elsewhere, there would be a greater use of micropore by NO. This appears to be inconsistent with the data.

There is also a possible role of mineral catalysis in defining active sites. Wyodak coal contains 6.3% ash, which contains a significant amount of calcium, see Table 1. Calcium is known to be a very good catalyst for gasification reactions⁵⁰⁻⁵². Therefore, the distribution of catalytic sites may influence significantly the porosity development as well. Hurt *et al.*⁹ even suggested that the catalytic sites may lie preferentially on the surfaces of meso- or macropores. It has also recently been clearly established that there is in some cases a good correlation between calcium surface area and NO reduction activity⁵³, better than the correlation of reactivity with BET surface area. That study showed the decrease in

CaO area with increasing burn-off, attributable to a decrease in catalyst dispersion, rather than calcium loss. The correlation with other samples was not as good, so this hypothesis cannot yet be considered as proven. Still, it has the potential for explaining why larger pores might seem to be more effective on the basis of their containing a larger fraction of active sites. This is an alternative hypothesis to that based on accessibility. This issue is being further examined.

3.2 Differences in Porosity Development in Different Gases

3.2.1 Introduction

Existence of kinetic control in a certain size range of pores does not rule out the possibility that a fraction of the pores may not be accessible to the reactant. That is to say, a correlation of reactivity with surface area does not assure that all measurable micropores can participate in reaction. Pores of different sizes may be utilized to different extents during the gasification reaction, possibly because of activated diffusion or totally precluded entry into very small pores (submicropores) or because of an uneven distribution of active sites among pores of different sizes. Large diameter reactant gas molecules may experience severe diffusional limitations in the submicropores. Another possibility is that active sites for a particular gas molecule may be found only in certain pore size ranges, and an uneven distribution of active sites will result in inhomogeneous utilization of different pores⁵⁴. These possibilities should not be confused with traditional "transport limitations", resulting in Zone II behavior.

It has been reported⁴⁴ that different gasification agents develop porosities differently: Steam produces more mesoporous carbons and CO₂ develops better microporosity, even when overall reactivity is quite comparable. Other results⁸ seem to indicate also that different porosities are developed in different oxidizing gases.

In one study²¹ it was claimed that small pores are not fully utilized during gasification with oxygen, whereas carbon dioxide penetrates into all pores. Dutta and Wen² found that surface area changes of different coal chars with conversion are much larger in O₂ than in CO₂. Similar results have been reported for steam and CO₂ gasification⁴², where higher surface areas are developed in steam than in CO₂ at the same temperature.

Our results showed that CO₂ developed much lower surface areas during gasification as compared with O₂ and NO at intermediate conversions, where surface area evolution is mainly governed by pore enlargement. This was true despite the selection of conditions which gave the same overall gasification rates in all three gases. There are several possible explanations for why this is so. The first, already mentioned above, is that different active sites are involved in each gas, and that the active site densities in the different pore sizes are not the same. The other which has been mentioned is a possibility that certain species cannot enter all of the available micropores. This seems to be less plausible for carbon dioxide, since it has been shown to actually be able to penetrate porosity closed to nitrogen. Alternatively, gasification can result in removal of cross-linking atoms allowing somewhat better alignment of small carbon crystallites to occur. This accelerates the normal annealing process which can occur thermally at higher temperatures. If one gasification agent is more effective at removal of key atoms (those holding crystallites apart) than is another, then there may be differences due to this effect as well.

3.2.2 Relative Reactant Penetration

To gain a better understanding of how deeply different gases can penetrate during gasification, pore size distributions (PSD) were determined from N₂ and CO₂ adsorption isotherms before and after gasification of a second type of carbon, a raw tire char. Raw tire char was used for this part of the study because it has a well developed mesoporosity, and a limited number of micropores. The nitrogen isotherms are shown in Figure 21, and the

BET area calculated from these data ($75 \text{ m}^2/\text{g}$) is comparable to, but lower than, that in the raw Wyodak char. The surface area obtained using carbon dioxide is comparable, so molecular sieving effects are not important in the raw tire char. One difference comes in the small microporosity itself. It is somewhat lower in the tire char than in the Wyodak char, as may be seen from a comparison of the isotherms near $P/P_0 = 0$. There is also a great deal more large porosity in the tire char, as revealed by the adsorption volumes near $P/P_0=1$.

The nitrogen PSD of the raw tire char is given in Figure 22 and shows that before gasification there exist pores ranging in size from micropores to macropores. After gasification in oxygen, as in the case of the Wyodak char, the PSD is similar in shape to the initial PSD, but the pore volume has increased significantly in all size ranges. Once again, the questions that may be raised relative to the ability of the BJH method to accurately portray the PSD do not alter this qualitative observation.

In contrast to this, gasification of tire char in NO and CO₂ increased only the volume of pores in the micro/mesopore peak between 10 and 100 Å. This suggests that NO and CO₂ cannot penetrate into the smaller micropores, and thus cannot grow these as can oxygen. There are obviously far too few data upon which to base a strong conclusion, and work on this point continues.

One additional piece of support for NO gasification reaction occurring mainly outside the micropores of tire char comes from the relatively constant value ($\pm 5\%$) of the average micropore size, calculated from N₂ adsorption isotherms, using the Dubinin theory of gas adsorption in micropores. Therefore, there is no clear indication of micropore widening which suggests that the penetration of reactants into micropores is limited even under intrinsic reaction rate control.

It is interesting to note that Karsner and Perlmutter⁵⁵ found that the oxidation rates of different coals were roughly proportional to the volume of pores of radius larger than 12 Å. Pore volume does not seem to be the correct factor to correlate reactivities, but similarities with our results are intriguing. Dutta *et al.*¹ observed that the rates of CO₂

gasification of their char were proportional to the surface area lying in pores larger than about 15 Å. Thus there have been other studies which have suggested that micropore accessibility issues could be playing a role in determining reactive surface area.

3.2.3 The effect of chemical reaction

The second factor that can affect the course of pore enlargement is the reaction mechanism on the char surface. As noted above, the ability of a reactant to attack at different points in the carbon structure determines what are termed “active sites”. Depending upon how these are distributed and which ones a particular reactant can make use of, pore enlargement can occur in different ways. Unfortunately, gasification reaction mechanisms have not been developed in any reliable detail. Active sites might include surface defects, edge atoms, sites next to mineral catalysts and even basal plane atoms, but precisely how these are attacked is not yet clear. As already noted, if catalytic sites are not distributed uniformly in different pore size ranges, then enlargement could occur differently in different size ranges. Likewise, if certain types of reactions are sterically hindered (or promoted) in micropores, this could dictate a preference for reaction in one size range over another.

The thermochemistry of gasification reactions indicate another potential issue. The following thermochemical calculations show that NO and O₂ gasification reactions are exothermic, whereas CO₂ gasification is endothermic.



The exothermic reactions in NO and oxygen could produce a localized hot spot on the char surface, at which further reaction takes place more effectively. How this might influence pore enlargement or creation is unclear.

It would be expected that changes in temperature have important effect on surface area development. Usually higher surface areas are developed with decreasing gasification temperature^{39,42}. This is attributed to a balance between the rate of gasification and the rate of diffusion of reactant into the interior of the char. At lower gasification temperatures there is an increase in microporosity but mesoporosity is not developed; at higher gasification temperatures the micropores develop less, whereas there is an important increase in mesopores^{44,56}. In reactions showing multiple mechanism behavior even under Zone I conditions (such as NO or CO₂), it is unclear how temperature shifts might influence pore development.

3.3 .Pore diffusion control regime (Zone II)

Intraparticle diffusional limitations and low utilization of surface area associated with the micropores is characteristic of Zone II conditions. Reaction occurs mostly in the larger macropores and on the external surface under these conditions. Pore accessibility to reactants becomes a major factor in determining observed gasification rates. Walker⁵⁷ showed that in most coal chars in which all pores have a given length to diameter ratio the rate of gas transport into and out of the particle is limited by diffusion in the feeder pore system. Therefore, Zone II may be dictated by a feeder system of larger pore size. In actual practice, it is often difficult to observe Zone II behavior, as it occurs only over a narrow range of temperature. Often it appears as though transition occurs directly from Zone I to external transport control (Zone III).

3.3.1 Surface area and pore volume development in Zone II

The existence of zone II in NO gasification gives us a unique opportunity to study the porosity development under those conditions. In the pore diffusion limited regime gasification in the micropores is expected to be severely limited, therefore no large changes in surface area and pore volume are expected.

Nitrogen and argon BET surface area evolution curves for NO reaction in Zone II, shown in Figures 3 and 5, indicate that initially the surface area grows more slowly than in Zone I. Above 20% conversion the surface area remains relatively constant. The increase in surface area appears to be mostly due to opening of closed porosity, because the curve parallels that observed under Zone I conditions, but is lower. The increase is slower than in Zone I because gasification takes place only on accessible surface; some blocked pores within the interior of the particle cannot be opened up because the reactant NO simply cannot gain access to the blocking carbons. The observed surface areas in Zone II are on average two times smaller than those in Zone I for a comparable degree of burn-off, but it must be remembered that the carbon which is gasified is not coming from the same places under Zone I and Zone II conditions. Also it needs to be kept in mind that the increase in total surface area does not mean that the reactive surface area changes to the same degree. Pores which are opened up (from pre-existing closed porosity) may be of too limited accessibility to be involved in subsequent reaction.

Pore volumes, calculated from N₂ isotherms, increase almost linearly with burn-off, see Figure 4. Therefore, as reaction proceeds, it is demonstrated that the initially closed porous structure becomes more open. If reaction were to proceed according to a purely shrinking core model on a grain level, then we would expect pore volume to increase monotonically with burn-off.

It is important to note that the CO₂ adsorption data in Figures 6 and 7 show that micropore area and volume exceed the nitrogen values rather far into the burn-off process. This was not observed under Zone I conditions, under which the nitrogen areas quickly

became larger than the CO₂ areas. What this means is that there remain a significant number of pores which are blocked to nitrogen but not to carbon dioxide, simply because the blocking atoms have not yet been removed.

3.3.2 Changes in pore size distributions during gasification

As was emphasized above, in the pore diffusion limited regime gasification takes place on a limited subset of the total surface. Therefore less dramatic changes in micro- and mesopore volume are expected. Figure 23 shows the pore size distributions determined at different levels of burn-off in NO at 1027 K. The PSD's do not shift nearly as markedly as they do in Zone I (see Figure 12) until the burn-off reaches over 12%, suggesting that NO cannot penetrate as effectively into micro- and mesopores during the initial stages of burn-off. However, after 29% burn-off some changes in mesopore structure development can be observed. Thus the pattern observed in Zone I is significantly delayed, to much higher levels of burn-off, in Zone II.

3.3.3 Reactivity vs. burn-off curves

There are several models that describe the reactivities of chars in the pore diffusion limited regime^{21,26-28}, where it is assumed that only the accessible surface area participates in reaction (macropores in the particle interior are not initially available) and that internal porosity is not fully available for reaction.

In the intrinsic reaction rate regime it was believed that the changes in gasification reaction rates reflect to a large extent changes in the internal surface area. In the pore diffusion limited regime, the locus of reaction depends upon the temperature. Near the high temperature end of the Zone II regime, reaction takes place near the external surface of char, therefore, the reactivity curve should reflect the changes in the external surface.

The reactivity vs. burn-off curve in Zone II, shown in Figure 24, is very different from the curves in Zone I (Figure 15). The interesting feature of the data in Figure 24

occurs during first 10% of conversion, where the reactivity curve exhibits a small peak, which then rapidly decreases to give a relatively steady rate value. The rates exhibit very little change with conversion until reaching about 75% of burn-off, after which reaction rate slowly starts to approach to zero. The initial peak in the rate vs. burn-off curves may be due to irregularities (defects, surface roughness etc.) on the external surface. After the surface roughness is eaten up, the reactivity stays constant meaning that the reactive surface area per unit mass increases. At high levels of burn-off, the particles start to collapse and surface area starts to decrease. The plateau of constant reactivity in a plot of $\frac{1}{m_0} \frac{dm}{dt}$ (Figure 24), is a period of continually increasing reactivity with burn-off in a plot at $\frac{1}{m} \frac{dm}{dt}$ (Figure 25) and shows that accessible reactive surface continually increases with burn-off from 10 to about 60%. Again, this is not observed in the behavior of the N₂ BET area of Figure 3, which shows the surface to be relatively constant over this time.

Figure 26 shows variation of reactivity with N₂ BET surface area. It appears to confirm that reactivity does not depend upon internal surface area in a simple way. On the other hand, Figure 4 confirms a continual increase in pore volume, meaning that porosity is being enlarged. The total micropore area is again shown to be irrelevant, and the expected Zone II behavior involving a slower increase in pore volume with burn-off than in Zone I is confirmed.

We have found no other data on reactivity vs. burn-off behavior under clearly defined Zone II conditions in the literature. There exist, however, several models that describe the reaction in zone II, such as the shrinking core model and discrete model. These models do not predict the observed peak at low levels of burn-off. The discrete model²¹ predicts a sudden jump when the particle starts to break up due to the increase in external surface area. However, our experimental results show no obvious jump in reaction rate at higher conversions, but our TGA conditions may not involve break-up.

It is quite complicated to talk about reactivity vs. burn-off behavior in a diffusion limited zone, because as a reaction proceeds the initially closed porous structure becomes

more and more available even in zone II. Therefore, reaction may be in the pore diffusion limited regime only until a certain level of burn-off. The conditions under which restricted diffusion controls gasification, causing a limited participation of porous surface area, are not well established, except in the most idealized theoretical cases.

3.4 Improvement of transport models

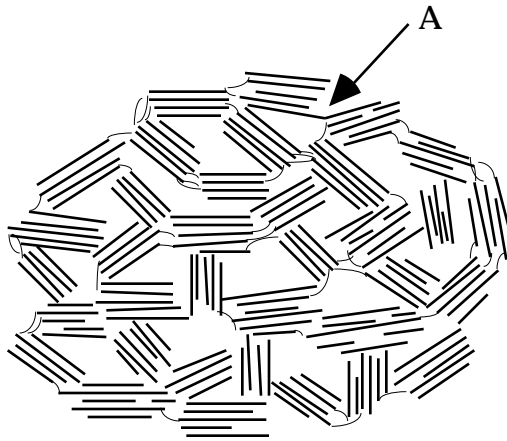
In a char, the morphology and porosity play a fundamental role in transport and reaction in the system. Recent theoretical studies have developed a number of models^{19,20,24} for these systems. The modeling of the evolution of the porosity or reactivity with burn-off is a complex task. The porosity development with burn-off involves several processes that take place simultaneously and many of the important steps are included in these transport models. However, the current study has experimentally recognized processes that are excluded from these models and these will be discussed in this section.

3.4.1 Opening of closed porosity

The total porosity of the carbon is not always accessible to reactant at low levels of burn-off because it is partially or totally blocked by the carbon deposited during pyrolysis or because some of the carbon crystallites form a closed structures. These new surfaces become available after a partial gasification (after about 1-2% burn-off in Wyodak char). It was recognized that opening of closed pores can be the main process of pore development during the first few percent of burn-off.

We know that the presently studied chars are non-graphitizable carbons, which means that there is no long range order of the graphitic units. Still, local ordering to an extent that depends on the heat treatment temperature, is expected. Considerable evidence for small structural units of about 40 Å size within char have been proposed⁵⁸. In non-graphitizable carbons the porous structure is formed by strong cross-linking of structural

units, which leads to a random orientation of the crystallites. The short range order guarantees the presence of slit-shaped micropores. This model is similar to that proposed by Franklin^{59,60} and used also by Kaneko *et al.*⁶¹. Similar structural units are the building blocks for the theoretical model proposed by Kantorovich and Bar-Ziv²⁴, where the microporosity of highly porous carbons is built from microcrystals (microrods). The gasification of this structure is assumed to take place preferentially near the joints of microcrystals. The rate of oxidation of carbon crystallites is generally thought to be much faster in the direction parallel to the basal planes (along their edges) than perpendicular to them. Therefore, it would be expected that during the initial stages of gasification, some of the closed porosity will be opened. Consider the fact that new porosity can be opened in the following structural model, if a limited amount of attack takes place near the point marked A.



The model proposed by Kantorovich and Bar-Ziv²⁴ does not consider the possibility of pore opening, because they based their model on highly porous activated carbon where all porosity is accessible. In most practical gasification processes, however, the "virgin" chars have a great deal of closed porosity. Therefore, this additional step should be added to all transport/reaction models. The largest degree of pore opening seems to take place through the removal of a small percentage of key blocking atoms between microcrystals.

3.4.2 Limited use of microporosity

In discussions of gasification mechanisms and models the assumption that all of the surface area is available for reaction seems to be an overestimate. It was shown experimentally⁹ that the CO₂ gasification reaction may take place primarily outside the microporous network of subbituminous coal char. This was explained by a higher concentration of active sites (primarily catalytic sites) on larger pore surfaces.

Our results indicate the limited development of micropores during gasification in carbon dioxide. An initial increase in surface area with burn-off, due to opening of closed pores, was observed but it was not as large as in O₂ or NO at comparable overall reaction rates. If the micropores are fully utilized in gasification, then one would expect a similar increase in micropore surface area at intermediate levels of burn-off. Therefore, this suggests that the use of micropore surface area during gasification may be limited in CO₂ gasification. On the other hand, the kinetic data obtained for carbon dioxide gasification showed that what micropore area there was, seemed to be utilized (Figure 17). Thus there remains a question as to why carbon dioxide can utilize the surface area, but it cannot open it up as effectively. On the other hand, the clearer example of the potentially limited use of micropores was provided by the reaction rate of NO in Zone I.

Transport models should set a limit into which pores gases can diffuse, where the limiting pore diameter should be different for different oxidizing gases. The random pore model by Gavalas¹⁹ is one of the few models that include the limited use of micropores (smaller than 6 Å by their definition) into their model. It was assumed that the diffusion in micropores is so slow that the micropore surface area makes a constant contribution to the reaction rate, whereas the surface area in larger pores is exposed to a uniform concentration of reactant gas.

3.4.3 Different oxidizing gases develop different porosities

The different porosity development by different oxidizing gases was described by Rodríguez-Reinoso⁴⁴, where steam developed higher mesoporosities and CO₂ developed more micropores. Our results showed that O₂, CO₂ and NO developed different porosities under conditions at which intrinsic reactivities were similar.

It was suggested that the smallest pores into which different gases can penetrate were different and that O₂ appeared to be able to penetrate porosity more effectively than CO₂ or NO. However, this does not mean that surface area development follows the same order. It was shown that NO developed higher surface areas than CO₂, even where the NO gasification reaction took place in larger pores.

This suggests that transport models should take into account the possibility that different oxidizing gases develop different porosities even in the kinetic control regime at similar intrinsic reactivities. The different porosity development seems to be related to the distribution of active sites, where different active sites might be involved in different gasification reactions.

4. Conclusions

The conclusions drawn from this study are summarized as follows:

1. Porosity evolution with burn-off, in the kinetic control regime, depends upon several processes which take place simultaneously. At low levels of burn-off it is dominated by opening of closed porosity; at intermediate levels of burn-off, pore enlargement is the main process; at high levels of burn-off, collapse of the pore structure and possibly particle shrinkage, characterize the porosity development.
2. Different oxidizing gases develop different porosities in the kinetic control regime. NO gasification is effective in opening up closed porosity, but may be limited in its ability to enlarge very small micropores; oxygen gasification develops pores ranging from micro- to

macropores; CO₂ gasification appears to take place uniformly, but relatively smaller surface areas are developed, perhaps because of non-uniformity of active site distributions.

3. In the kinetic control regime, different oxidizing gases appear to be able to penetrate into different size pores. In particular, there is evidence to suggest that NO is limited in its ability to penetrate porosity.

4. In the pore diffusion control regime (Zone II), the development of porosity is not surprisingly quite different from that in Zone I.

5. Transport models must necessarily account for differences in different oxidizing gases, even when intrinsic reactivities are very similar.

6. A step involving the opening of closed porosity must be included into transport/reaction models.

References

1. Dutta, S., Wen, C.Y., and Belt, R.J., *Ind. Eng. Chem. Process Des. Dev.*, **16**, 20, (1977).
2. Dutta, S., and Wen, C.Y., *Ind. Eng. Chem. Process Des. Dev.*, **16**, 31, (1977).
3. Mahajan, O.P., Yarzab, R., and Walker, P.L., Jr., *Fuel*, **57**, 643, (1978).
4. Tseng, H.P., and Edgar, T.F., *Fuel*, **63**, 385, (1984).
5. Tseng, H.P., and Edgar, T.F., *Fuel*, **64**, 373, (1985).
6. Su, J.-L., and Perlmutter, D.D., *AIChE J.*, **31**, 973, (1985).
7. Adschiri, T., and Furusawa, T., *Fuel*, **65**, 927, (1986).
8. Ballal, G., and Zygourakis, K., *Ind. Eng. Chem. Res.*, **26**, 1787, (1987).
9. Hurt, R.H., Sarofim, A.F., and Longwell, J.P., *Fuel*, **70**, 1079, (1991).
10. Hurt, R.H., Sarofim, A.F., and Longwell, J.P., *Energy & Fuel*, **5**, 290, (1991).
11. Senneca, O., Russo, P., Salatino, P., and Masi, S., *Carbon*, **35**, 141, (1997).
12. Hurt, R.H., Dudek, D.R., Longwell, J.P., and Sarofim, A.F., *Carbon*, **26**, 433, (1988).
13. Sahim, M., Gavalas, G.R., and Tsotsis, T.T., *Chem. Eng. Sci.*, **45**, 1443, (1990).
14. Petersen, E.E., *AIChE J.*, **3**, 443, (1957).
15. Szekely, J., and Evans, J.W., *Chem. Eng. Sci.*, **25**, 1091, (1970) and **26**, 1901, (1971).
16. Hashimoto, K., and Silveston, P.L., *AIChE J.*, **19**, 259, (1973).
17. Simons, G.A., and Finson, M.L., *Combust. Sci. Tech.*, **19**, 227, (1979).
18. Simons, G.A., *Combust. Sci. Tech.*, **19**, 217, (1979).
19. Gavalas, G.R., *AIChE J.*, **26**, 577, (1980).
20. Bhatia, S.K., and Perlmutter, D.D., *AIChE J.*, **26**, 379, (1980).
21. Sandmann, C.W., and Zygourakis, K., *Chem. Eng. Sci.*, **41**, 733, (1986).
22. Bhatia, S.K., *AIChE J.*, **33**, 1707, (1987).
23. Ballal, G., and Zygourakis, K., *Ind. Eng. Chem. Res.*, **26**, 911, (1987).
24. Kantorovich, I.I., and Bar-Ziv, E., *Comb. & Flame*, **97**, 61, (1994).
25. Kantorovich, I.I., and Bar-Ziv, E., *Comb. & Flame*, **97**, 79, (1994).
26. Hashimoto, K., Silveston, P.L., *AIChE J.*, **19**, 268, (1973).
27. Simons, G.A., *Comb. Sci. and Technol.*, **20**, 107, (1979).
28. Gavalas, G.R., *Comb. Sci. and Technol.*, **24**, 197, (1981).
29. Vorres, K.S., in *Users Handbook for the Argonne Premium Coal Sample Program*, ANL/PCSP-93/1, Argonne National Laboratory, USDOE, (1993).
30. Barrett, E.P., Joyner, L.G., and Halenda, P.P., *J. Chem. Soc.*, **73**, 373, (1951).

31. Olivier, J.P, Conklin, W.B., and Szombathely, M.V., In *Characterization of Porous Solids*, (Edited by Rouquerol, J., Rodríguez-Reinoso, F. Sing, K.S.W., and Unger, K.K.) pp. 81-89, Elsevier, Amsterdam (1994).
32. Gregg, S.J., Sing, K.S.W., *Adsorption, Surface Area and Porosity*, 2nd ed., Academic Press, London, (1982).
33. Marsh, H., and Wynne-Jones, W.T.K., *Carbon*, **1**, 269, (1964).
34. Debelak, K.A., and Schrodt, J.T., *Fuel*, **58**, 732, (1979).
35. Teng, H., Suuberg, E.M., and Calo, J.M., *Energy & Fuels*, **6**, 398, (1992).
36. Sing, K.S.W., *Pure Appl. Chem.*, **54**, 2201, (1982).
37. Rodríguez-Reinoso, F., and Linares-Solano, A., In *Chemistry and Physics of Carbon*, Marcel Dekker, New York, Vol. 21, Ed. Thrower, P.A., pp. 1-146, (1988).
38. Marsh, H., and Rand, B., *Carbon*, **9**, 47, (1971), **9**, 63, (1971), and **9**, 79, (1971).
39. Walker, P.L., Jr., in "*Carbon and Coal Gasification*", NATO ASI Series E- No. 105 (Eds. Figueiredo, J.L., and Moulijn, J.A.), Martinus Nijhoff, Netherland, p. 1, (1986).
40. Wigmans, T., *Carbon* , **27**, 13, (1989).
41. van Heek, K.H., and Mühlen, H.-J., in "*Fundamental Issues in Control of Carbon Gasification Reactivity*"(Ed. by J. Lahaye and P. Ehrburger), Kluwer, Boston, p. 1, (1991).
42. Hashimoto, K., Miura, K., Yoshikawa, F., and Imai, I., *Ind. Eng. Chem., Process Des. Dev.*, **18**, 72, (1979).
43. Bar-Ziv, E., in "*Fundamental Issues in Control of Carbon Gasification Reactivity*"(Ed. by J. Lahaye and P. Ehrburger), Kluwer, Boston, p. 79, (1991).
44. Rodríguez-Reinoso, F., in "*Fundamental Issues in Control of Carbon Gasification Reactivity*" (Ed. by J. Lahaye and P. Ehrburger), Kluwer, Boston, p. 533, (1991).
45. Verma, S.K., and Walker, P.L., Jr., *Carbon*, **28**, 175, (1990).
46. Ballal, G., and Zygourakis, K., *Chem. Eng. Comm.*, **49**, 181, (1986).
47. Moulijn, J.A., and Kapteijn, F., *Carbon*, **33**, 1155, (1995).
48. Smith, I.W., *Fuel*, **57**, 409, (1978).
49. Aarna, I., and Suuberg, E.M., *Fuel*, **76**, 475, (1997).
50. Linares-Solano, A., Salinas-Martínez de Lecea, C., Cazorla-Amorós, D., Joly, J.P., and Charcosset, H., *Energy & Fuels*, **4**, 467, (1990).
51. Cazorla-Amorós, D., Linares-Solano, A., Salinas-Martínez de Lecea, C., and Joly, J.P., *Carbon*, **29**, 361, (1991).
52. Illán-Gómez, J.M., Linares-Solano, A., Radovic, L.R., and Salinas-Martínez de Lecea, C., *Energy & Fuels*, **9**, 112, (1995).

53. Guo, F. and Hecker, W.C., *26th Symp. (Int.) on Comb.*, p. 2251, The Combustion Institute, Pittsburgh, 1996.
54. Sandmann, C.W., and Zygourakis, K., *Chem. Eng. Comm.*, **58**, 139, (1987).
55. Karsner, G.G., and Perlmutter, D.D., *AIChE J.*, **27**, 170, (1981).
56. Berger, J., Siemieniowska, T., and Tomkov, K., *Fuel*, **55**, 9, (1976).
57. Walker, P.L., Jr., *Fuel*, **59**, 809, (1980).
58. Born, M., and Klose, E., *Fuel*, **62**, 483, (1983).
59. Franklin, R.E., *Acta. Cryst.*, **4**, 253, (1951).
60. Franklin, R.E., *Proc. Roy. Soc.*, **A209**, 196, (1951).
61. Kaneko, K., Ishii, C., Ruike, M., and Kuwabara, H., *Carbon*, **30**, 1075, (1992).

Table 1. Chemical analysis of Wyodak coal.

	Wyodak coal
<u>Proximate analysis, wt%</u>	
Moisture	28.09
Volatile matter	32.17
Ash	6.31
Fixed carbon	33.42
<u>Ultimate analysis, wt% (moisture and ash free)</u>	
Carbon	75.01
Hydrogen	5.35
Sulfur	0.47
Nitrogen	1.12
Oxygen	18.02
<u>Mineral analysis of ash, wt%</u>	
Silicon dioxide	28.7
Aluminum oxide	15.5
Calcium oxide	15.1
Ferric oxide	10.2
Sulfur trioxide	22.0
Sodium oxide	1.5
Potassium oxide	0.8
Magnesium oxide	3.6

Table 2. Important parameters used in calculations of surface area and pore size distribution.

Parameters	Nitrogen	Carbon Dioxide	Argon	Carbon
Adsorbate Temperature [K]	77.4	195	77.4	-
Cross Sectional Area [$\text{\AA}^2/\text{molecule}$]	16.2	21.0	14.2	-
Liquid Density [g/cm^3]	0.808	1.1	1.4	-
Average Diameter [\AA]	3.0	2.8	3.36	-
Polarizability [$\text{cm}^3/\text{molecule}$]	$1.46 \cdot 10^{-24}$	$2.91 \cdot 10^{-24}$	$1.63 \cdot 10^{-24}$	$1.02 \cdot 10^{-24}$
Magnetic Suscept. [$\text{cm}^3/\text{molecule}$]	$2.0 \cdot 10^{-29}$	$3.9 \cdot 10^{-29}$	$3.25 \cdot 10^{-29}$	$13.5 \cdot 10^{-29}$
Surface Tension [erg/cm^2]	8.85	18.52	13.2	-
Nonideality	$6.58 \cdot 10^{-5}$	$2.75 \cdot 10^{-5}$	$3.94 \cdot 10^{-5}$	-
Adsorbent Density [g/cm^3]	-	-	-	2.25

Data taken from:

Autosorb-1 User Manual, Quantachrome Co., Boynton Beach, FL, (1996).

CRC Handbook of Chemistry and Physics, 66th Edition, CRC Press, Inc., Boca Raton, FL, (1985).

Table 3. Comparison of the areas obtained with the three adsorption probes (N₂, Ar and CO₂) at 20% burn-off.

Adsorbate	NO (Zone I)	O ₂ (Zone I)	CO ₂ (Zone I)	NO (Zone II)
	[m ² /g]	[m ² /g]	[m ² /g]	[m ² /g]
Nitrogen	460	490	380	260
Argon	310	365	310	255
Carbon dioxide	415	385	310	315

Table 4. Comparison of the areas obtained with the three adsorption probes (N₂, Ar and CO₂) at 60% burn-off.

Adsorbate	NO (Zone I)	O ₂ (Zone I)	CO ₂ (Zone I)	NO (Zone II)
	[m ² /g]	[m ² /g]	[m ² /g]	[m ² /g]
Nitrogen	410	440	380	290
Argon	310	365	295	235
Carbon dioxide	270	270	210	250

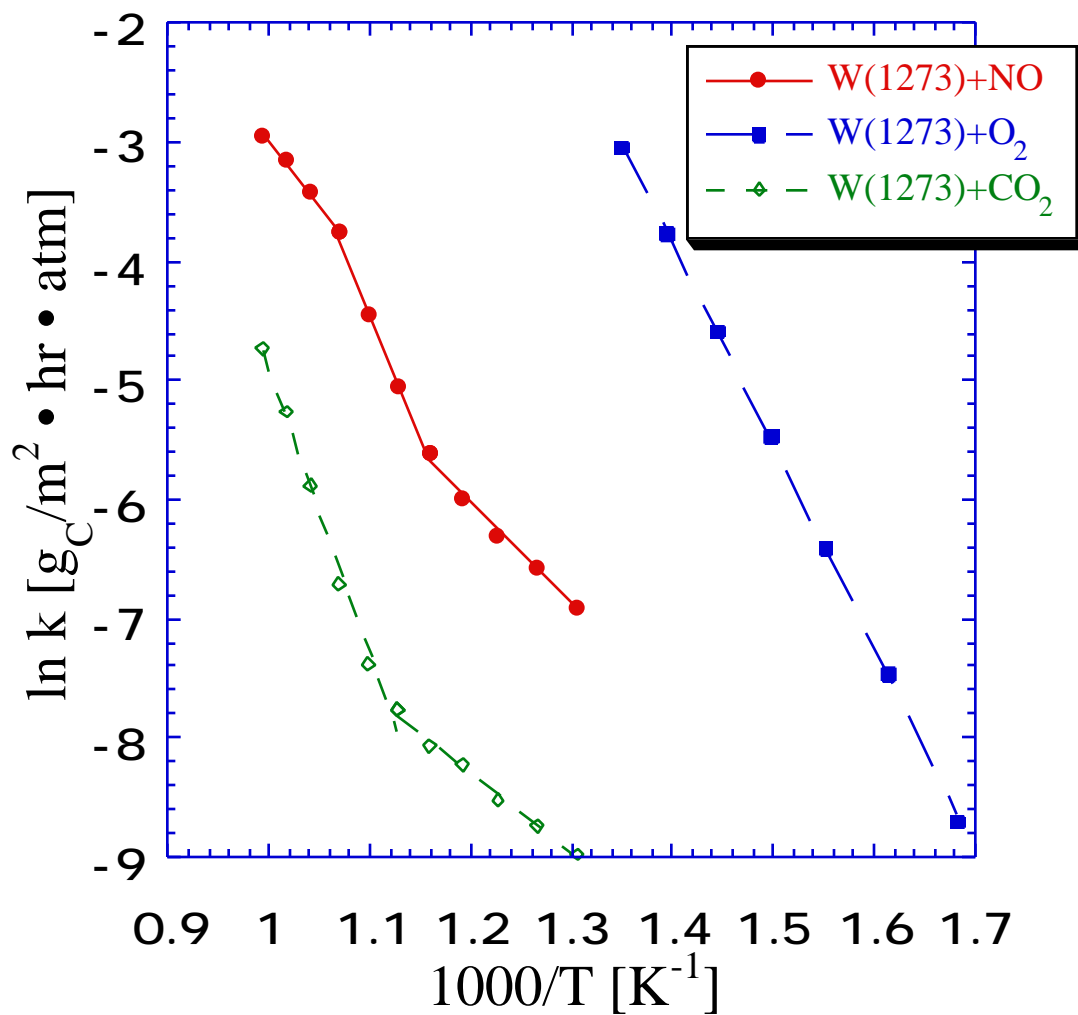


Figure 1. Reactivity of Wyodak coal char towards different oxidizing gases. The rate constants are expressed on a surface area basis. Measurements of reactivity were performed in a TGA. First order reaction was assumed with respect to the oxidizing gases. $P_{NO} = 0.82$ kPa, $P_{O_2} = 2.02$ kPa, $P_{CO_2} = 4.8$ kPa.

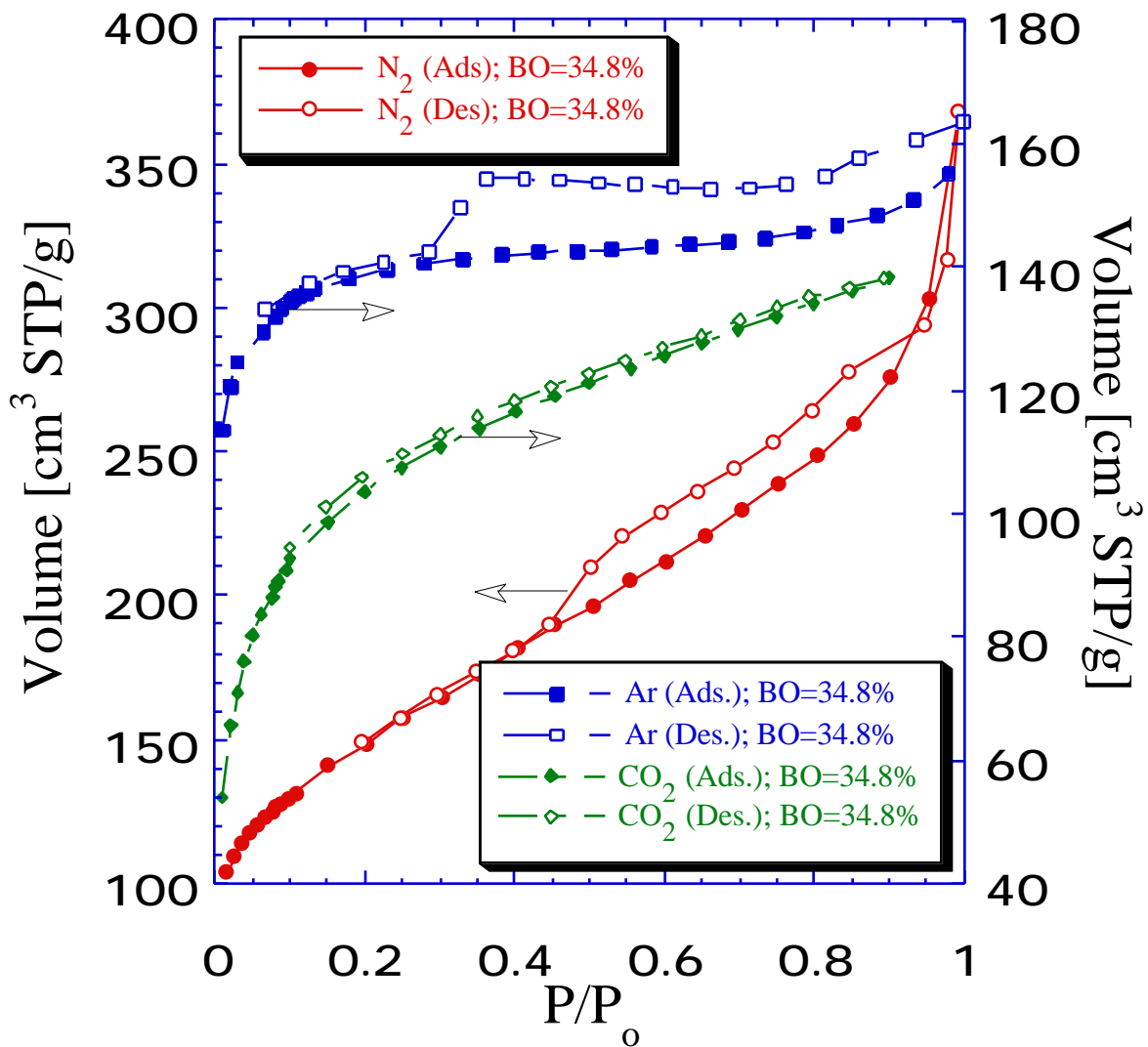


Figure 2. Nitrogen, argon and carbon dioxide adsorption isotherms on Wyodak coal char (burned-off to 29.4% in NO at 911 K). Solid symbols - adsorption isotherms; open symbols - desorption isotherms.

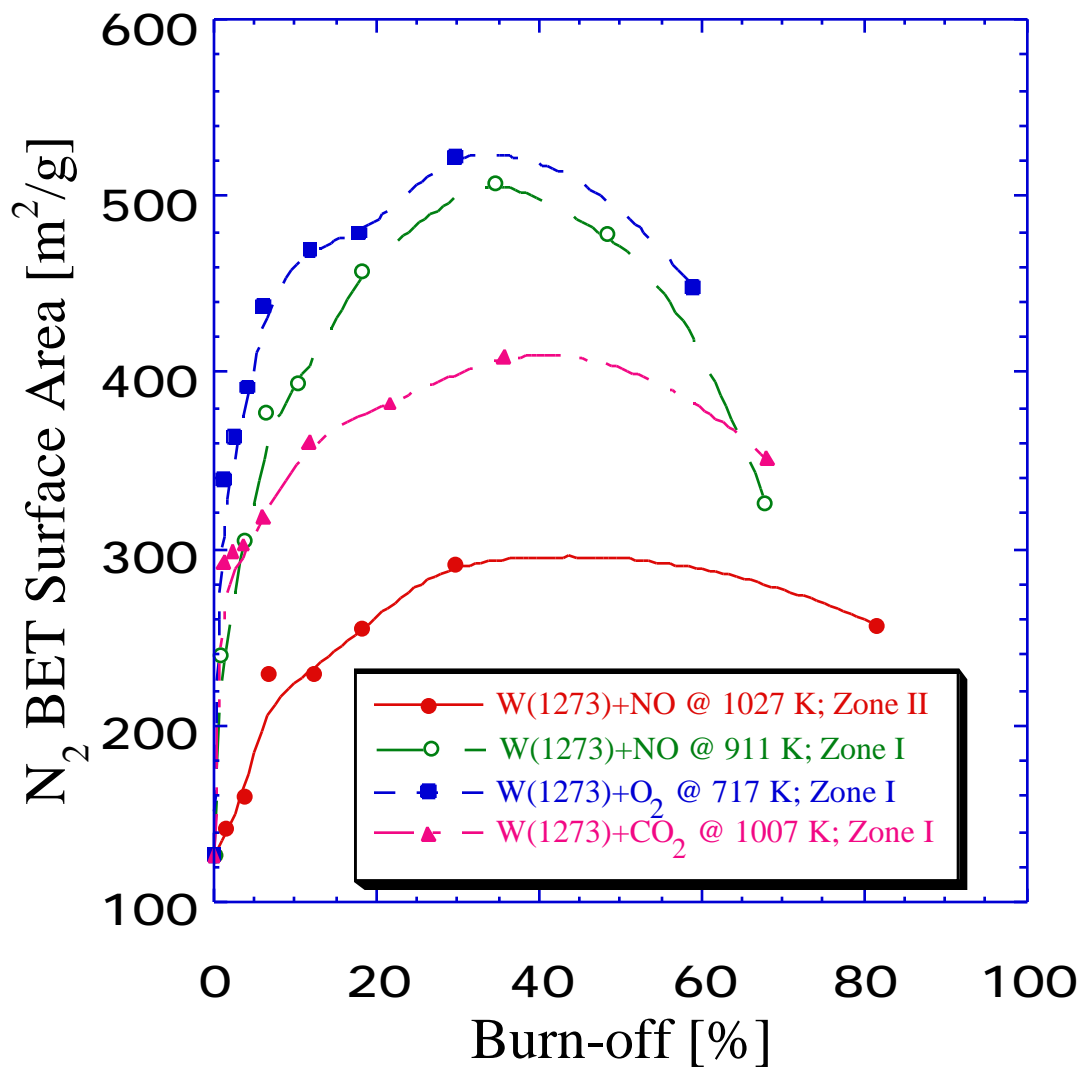


Figure 3. Wyodak coal char surface area evolution in different oxidizing gases and at different temperatures. Surface areas were determined from N₂ adsorption isotherm at 77 K using a BET theory.

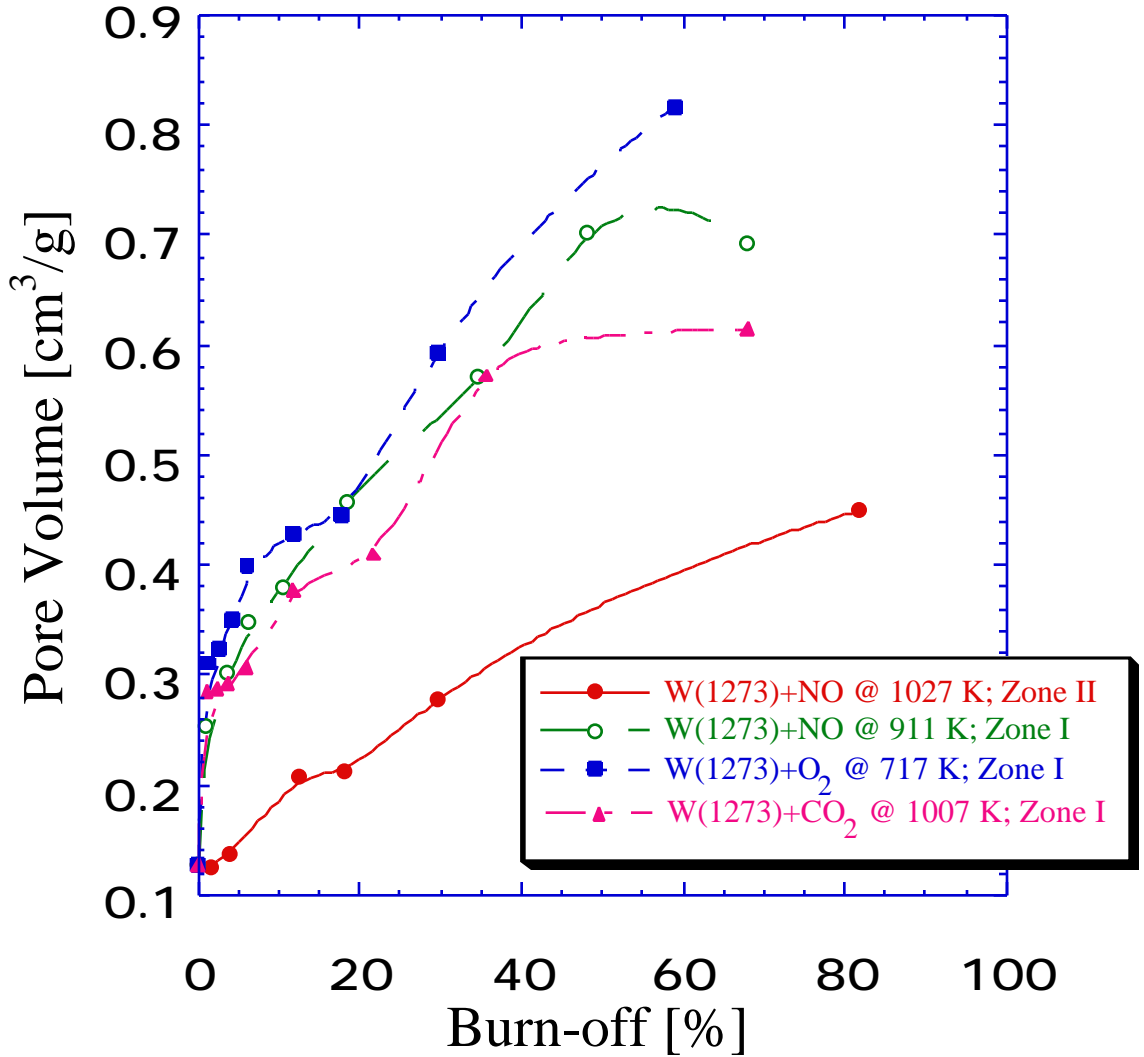


Figure 4. Wyodak coal char pore volume evolution in different oxidizing gases and at different temperatures. Total pore volumes were determined from N₂ adsorption isotherm at P/P₀= 0.995.

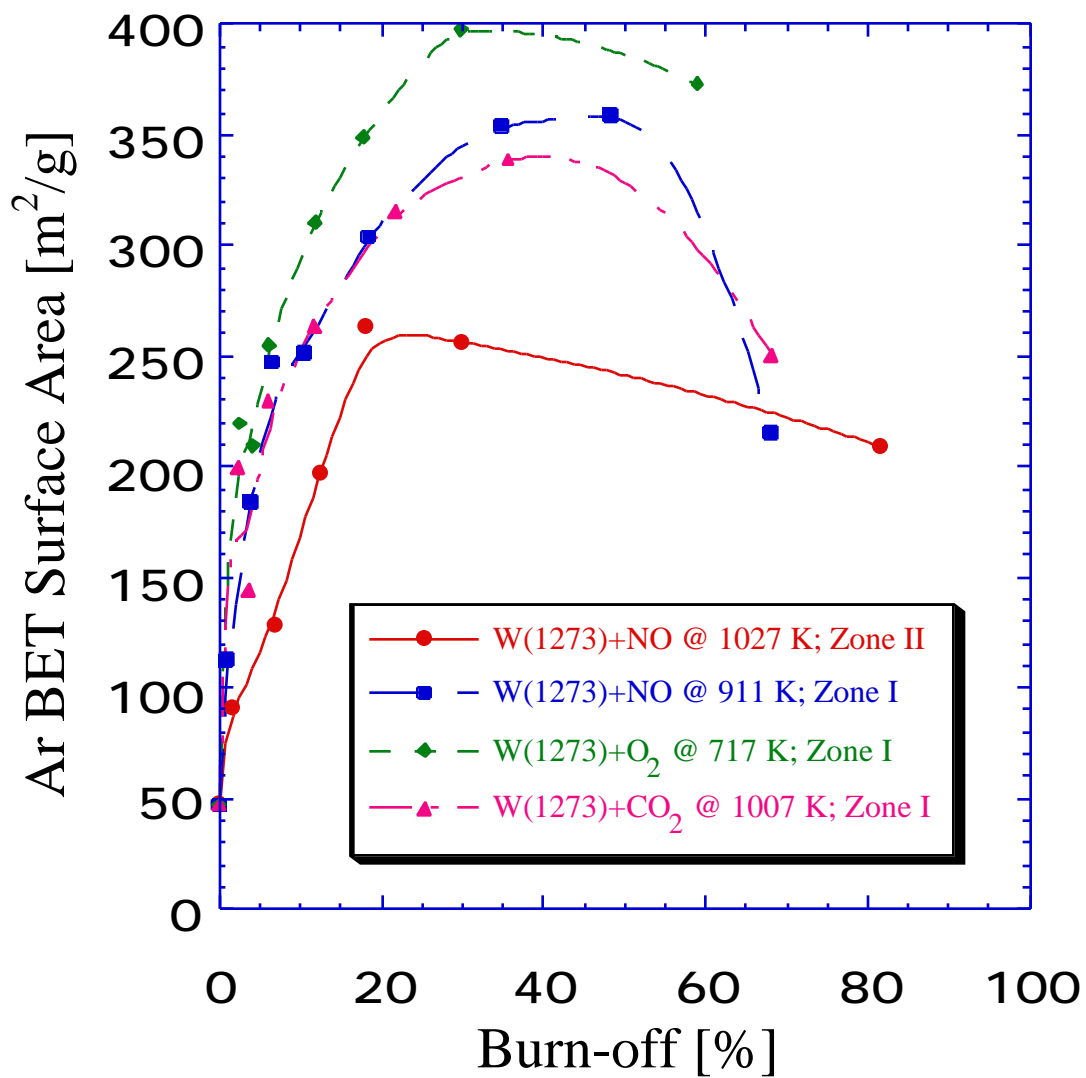


Figure 5. Wyodak coal char surface area evolution in different oxidizing gases and at different temperatures. Surface areas were determined from Ar adsorption isotherm at 77 K using a BET theory.

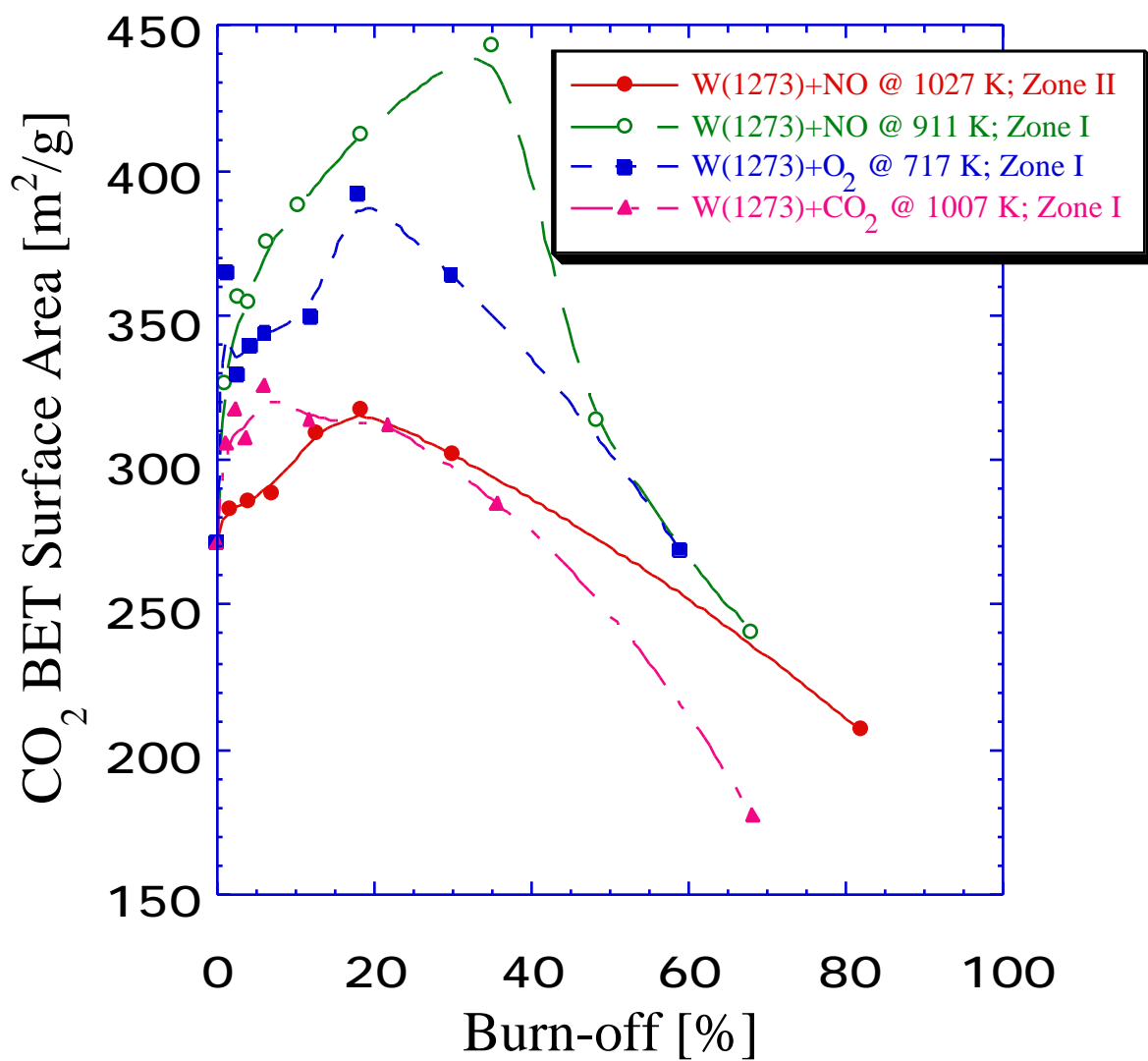


Figure 6. Wyodak coal char surface area evolution in different oxidizing gases and at different temperatures. Surface areas were determined from CO₂ adsorption isotherm at 195 K using a BET theory.

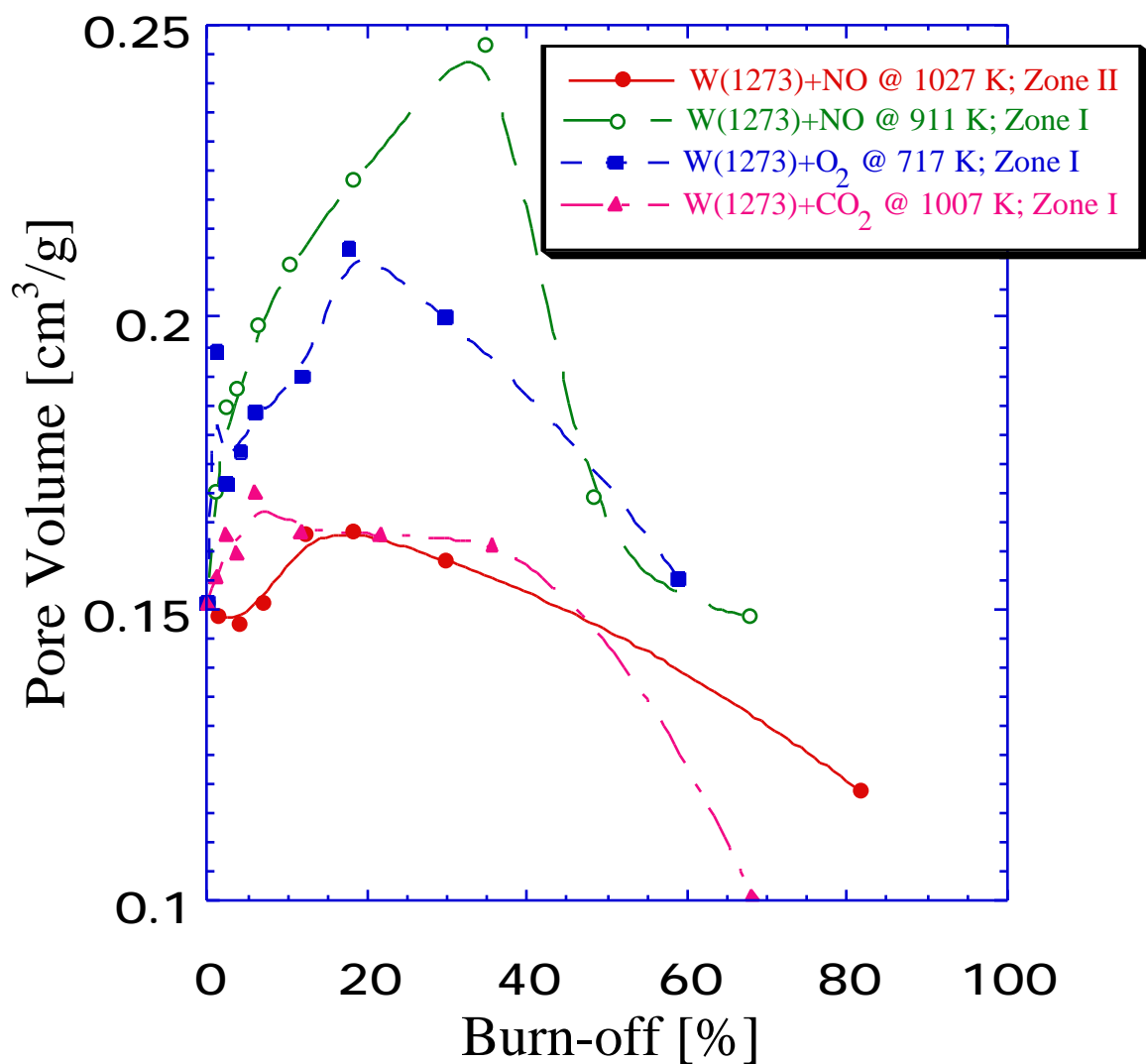


Figure 7. Wyodak coal char pore volume evolution in different oxidizing gases and at different temperatures. Total pore volumes were determined from CO₂ adsorption isotherm at $P/P_0 = 0.90$.

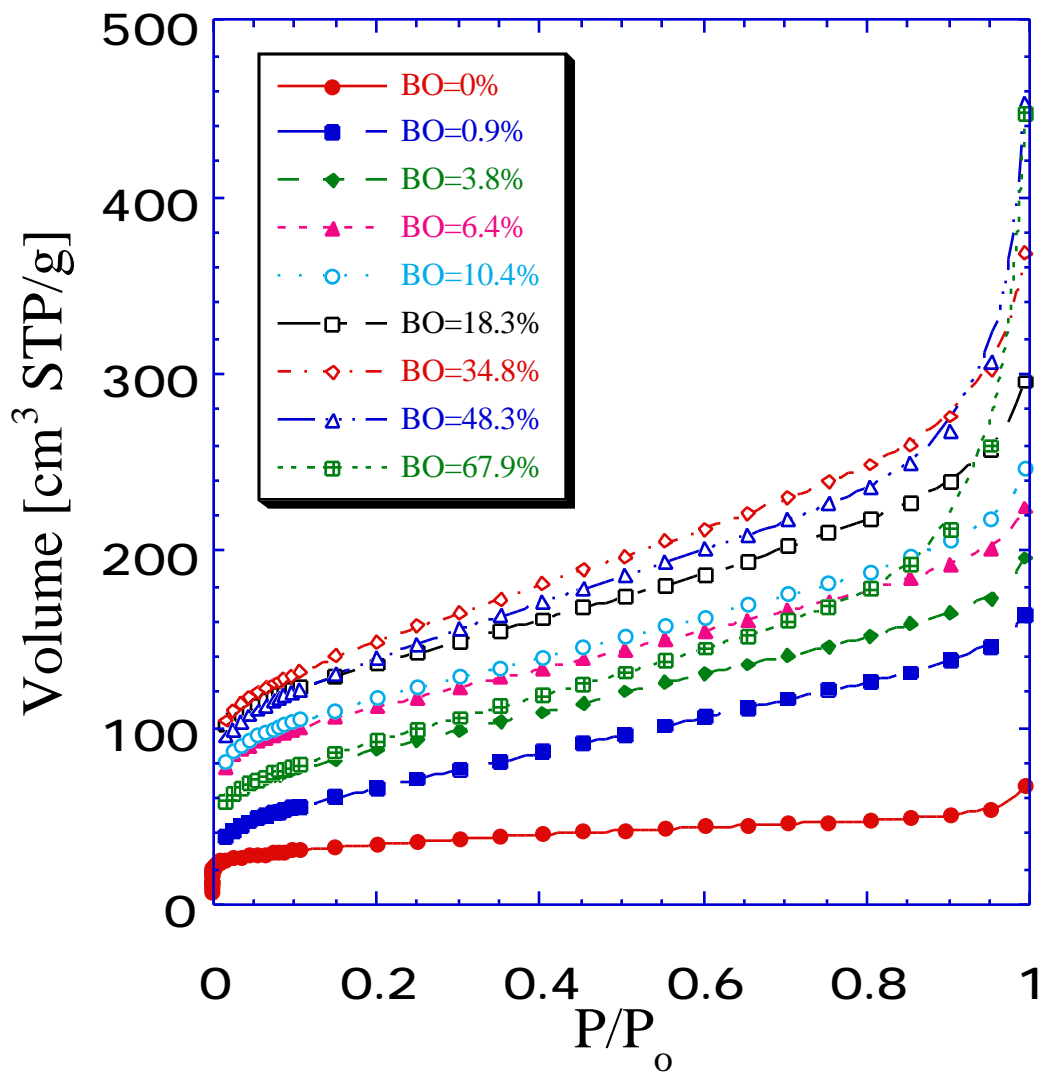


Figure 8. Nitrogen adsorption isotherms on Wyodak coal char determined at different levels of burn-off in NO at 911 K.

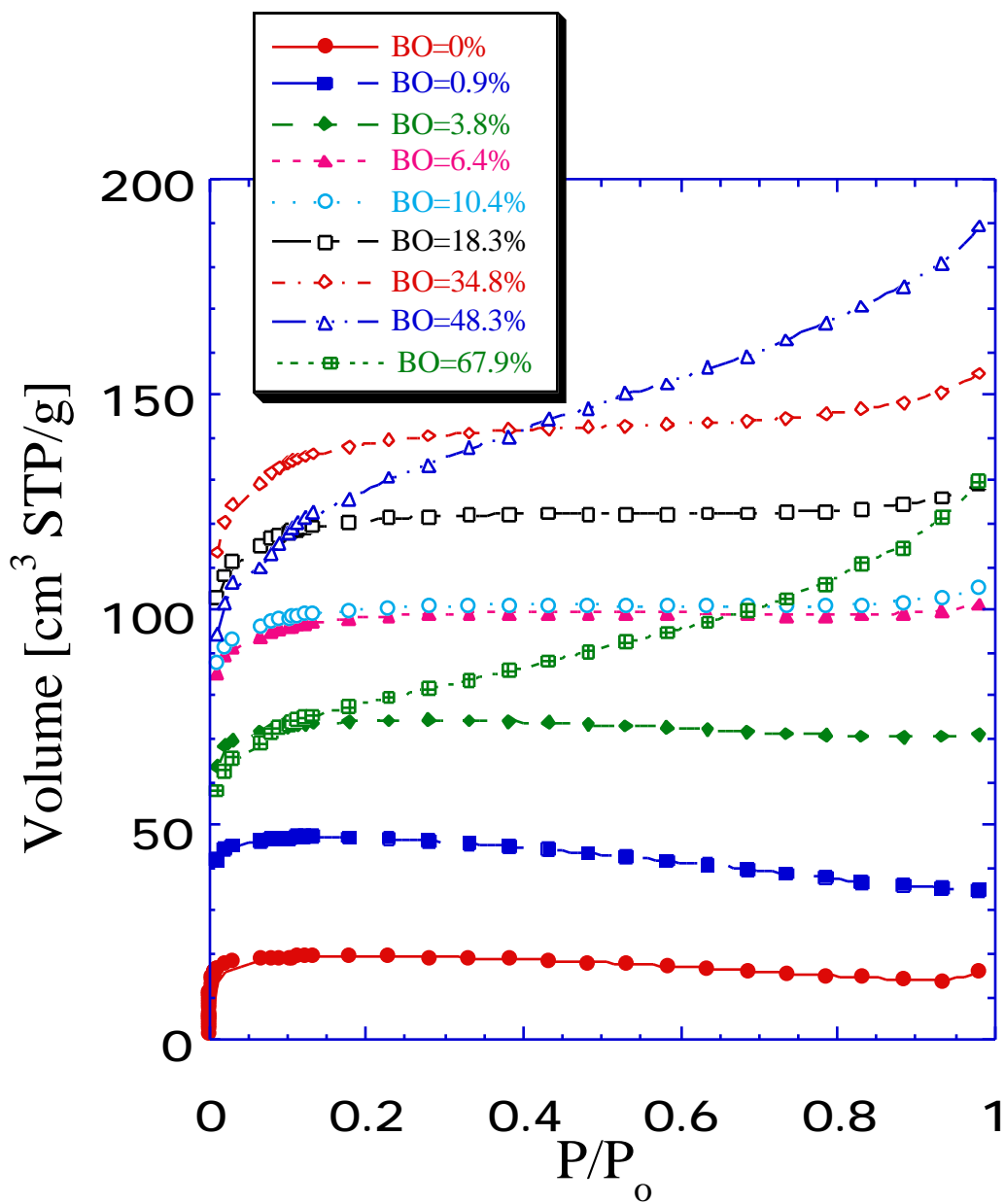


Figure 9. Argon adsorption isotherms on Wyodak coal char determined at different levels of burn-off in NO at 911 K.

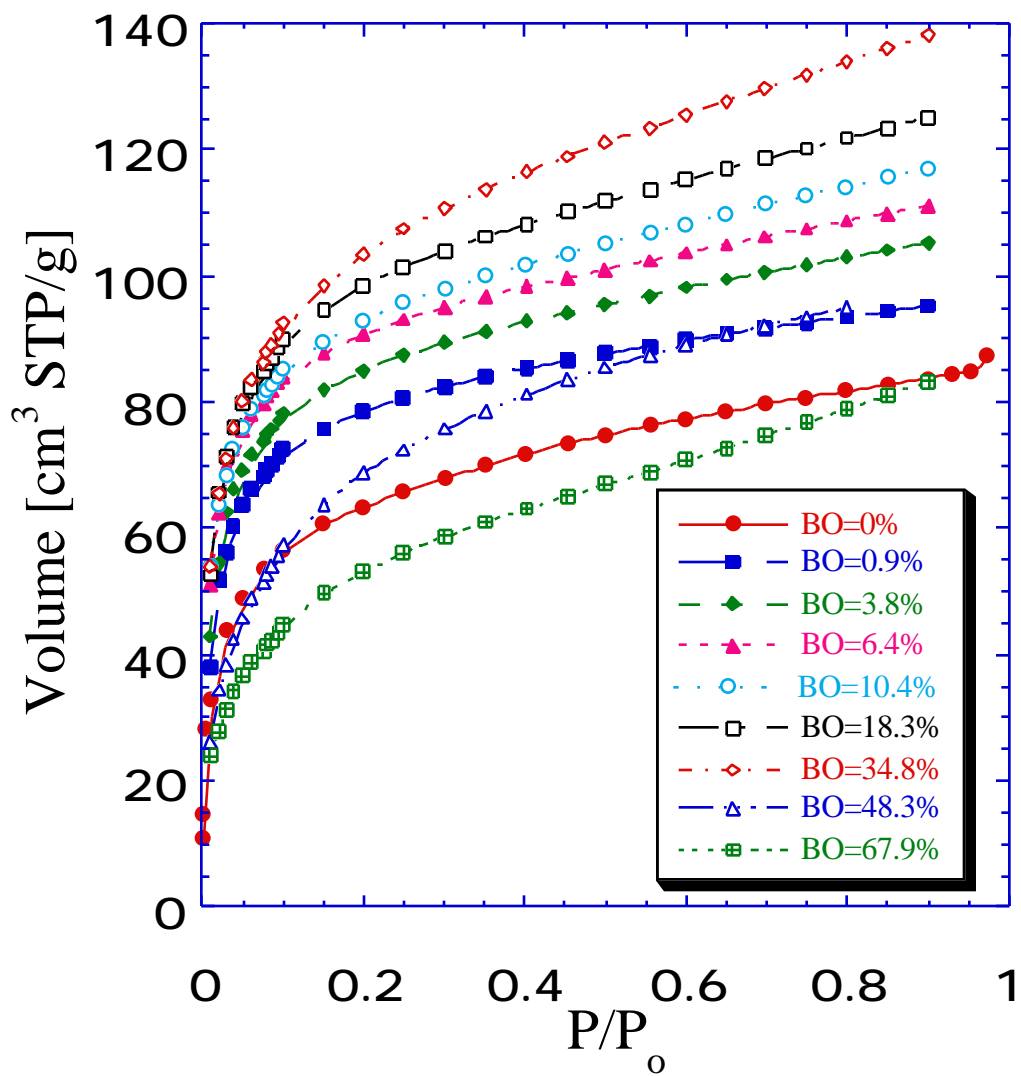


Figure 10. Carbon dioxide adsorption isotherms on Wyodak coal char determined at different levels of burn-off in NO at 911 K.

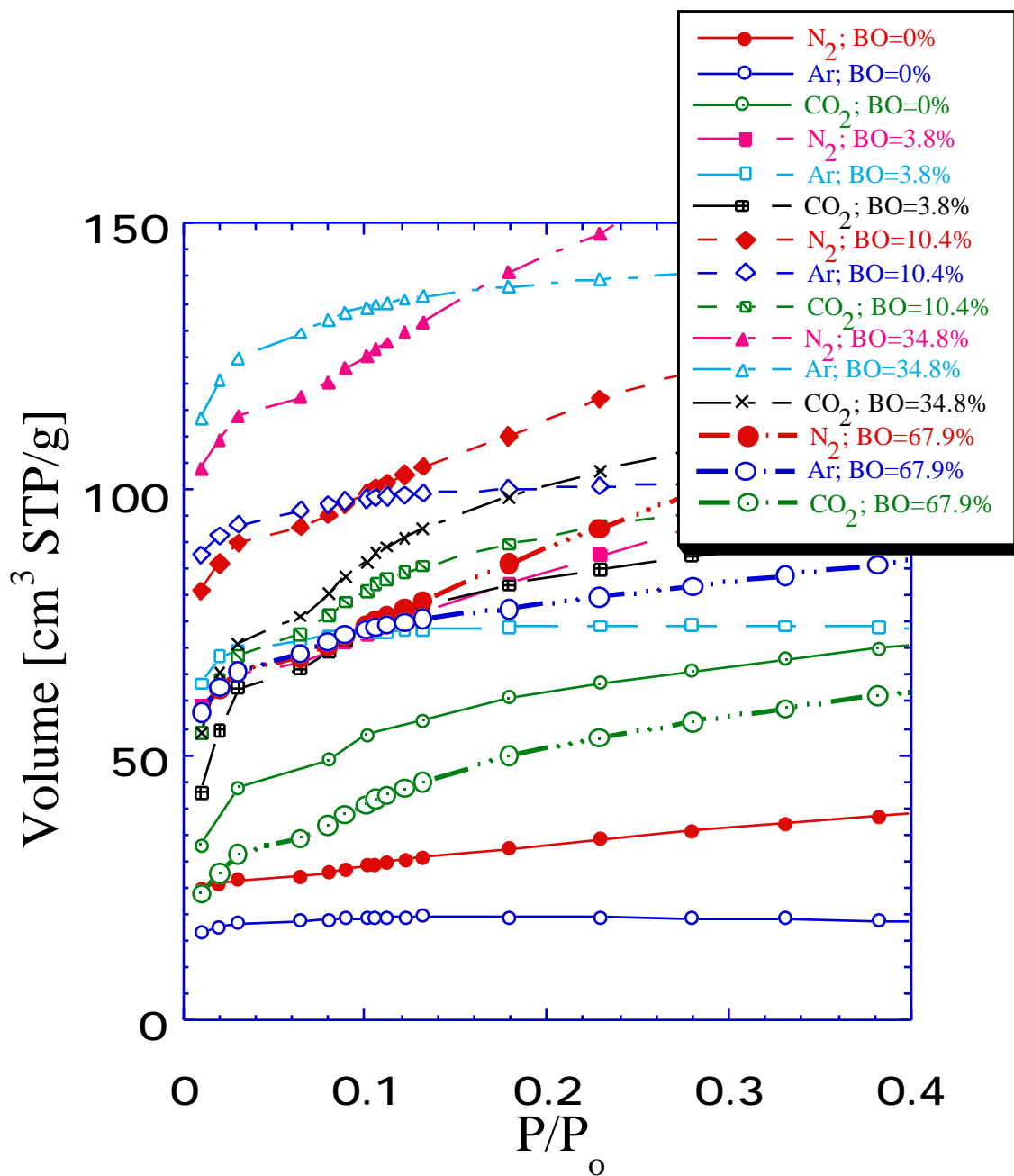


Figure 11. Comparison of the low pressure end of N₂, Ar and CO₂ adsorption isotherms on Wyodak coal char determined at different levels of burn-off in NO at 911 K.

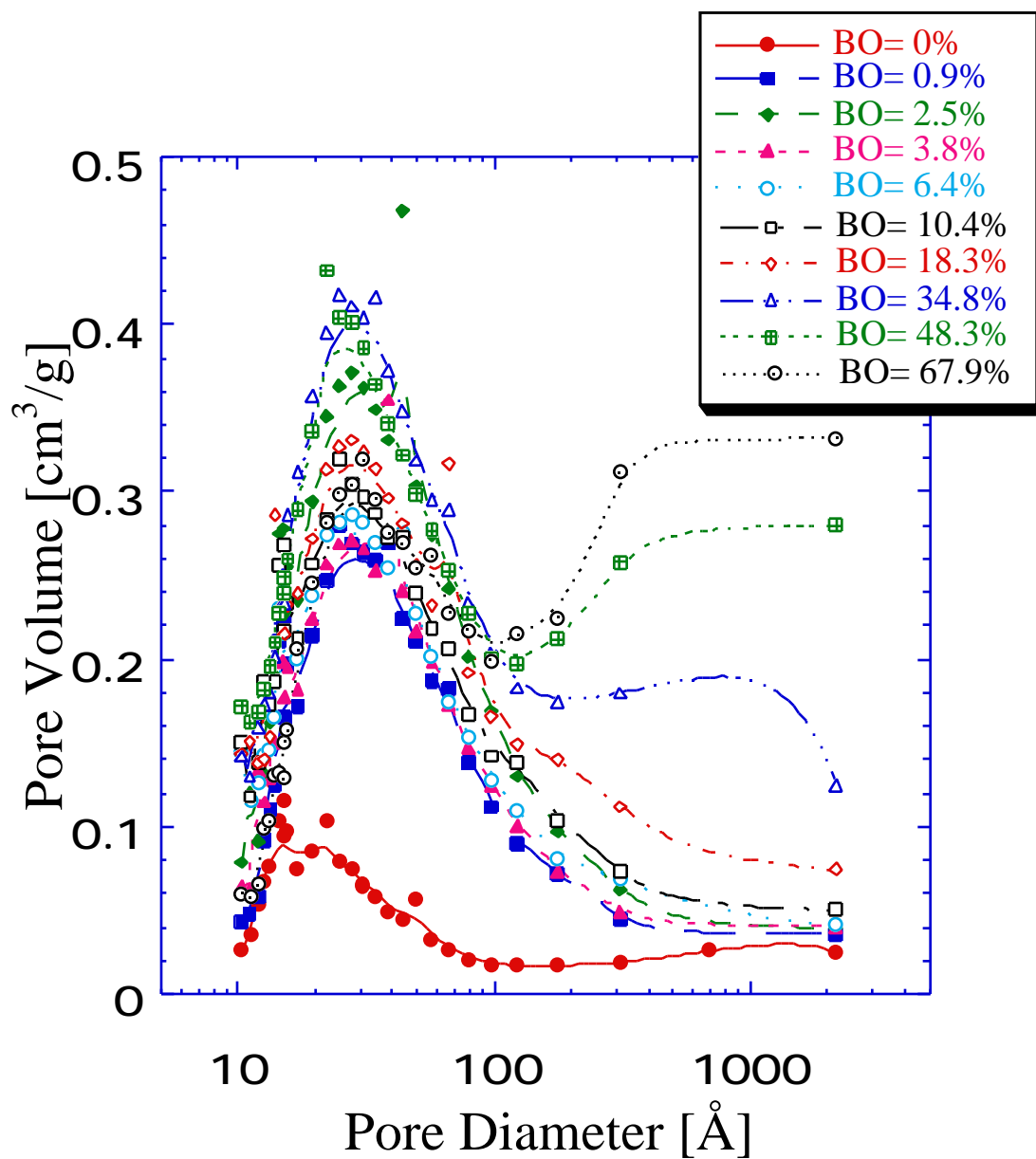


Figure 12. BJH pore size distribution for Wyodak coal char determined at different levels of burn-off in NO (Zone I). Samples were prepared in 0.82 kPa of NO at 911 K. Data from adsorption branch of N₂ isotherm.

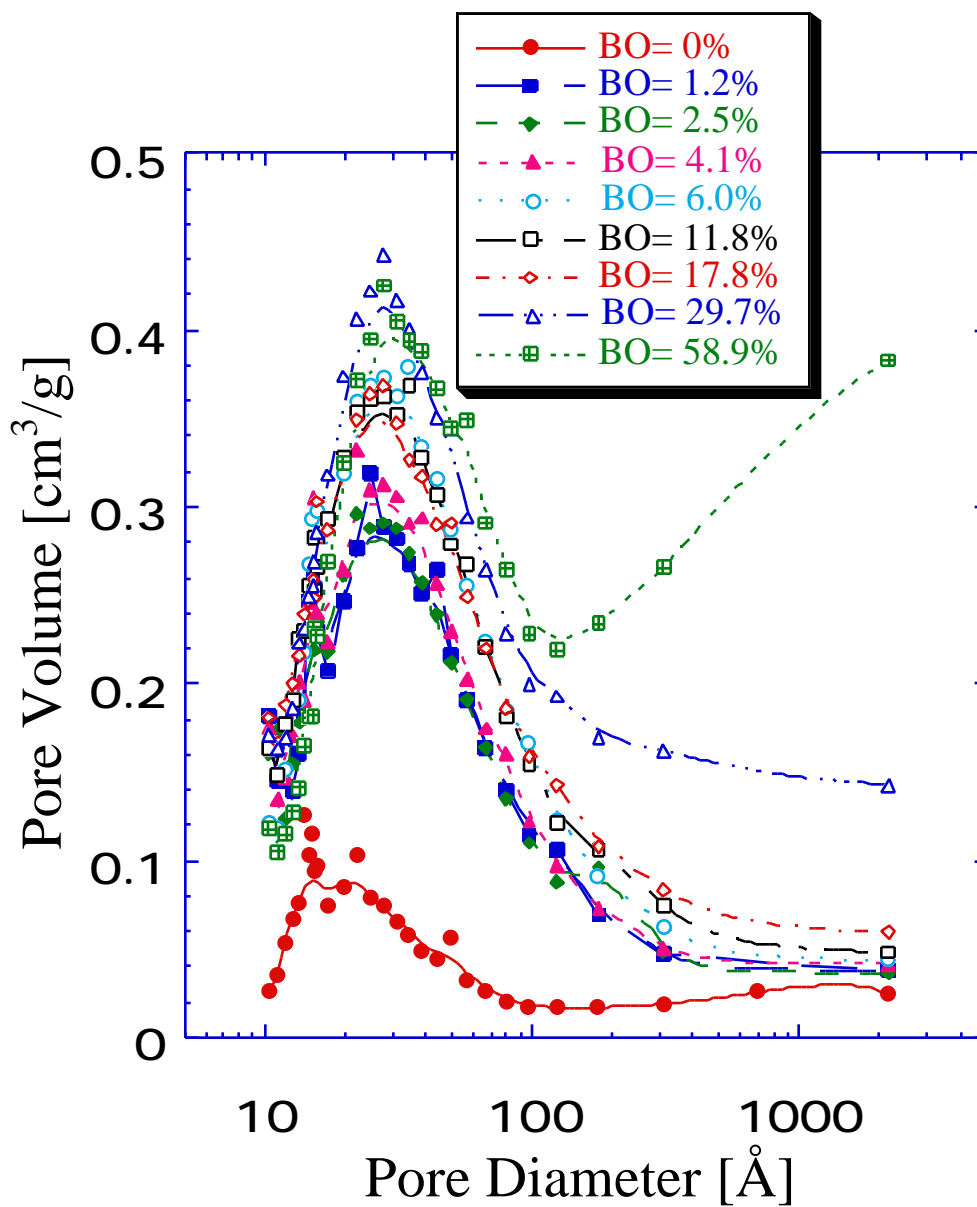


Figure 13. BJH pore size distribution for Wyodak coal char determined at different levels of burn-off in O₂ (Zone I). Samples were prepared in 2.02 kPa of O₂ at 717 K. Data from adsorption branch of N₂ isotherm.

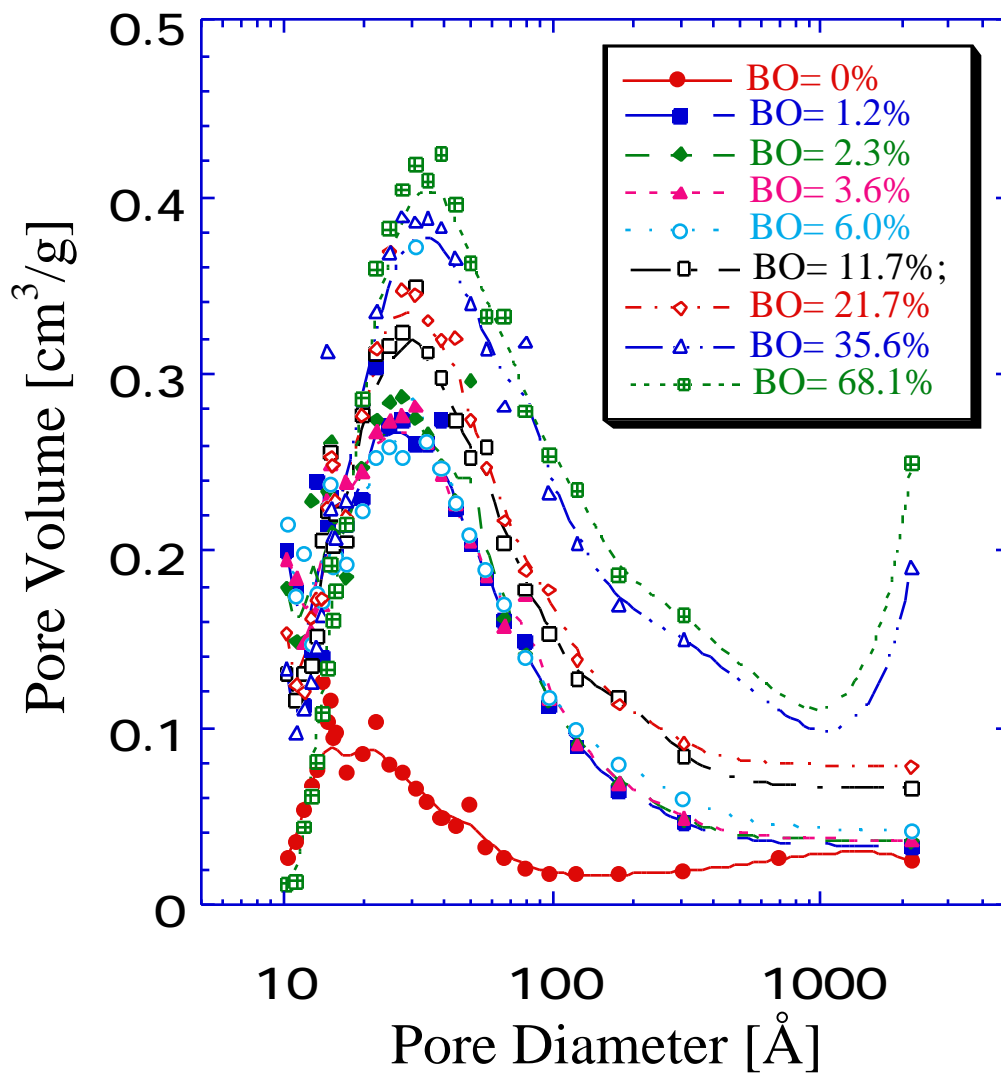


Figure 14. BJH pore size distribution for Wyodak coal char determined at different levels of burn-off in CO₂ (Zone I). Samples were prepared in 4.8 kPa of CO₂ at 1007 K. Data from adsorption branch of N₂ isotherm.

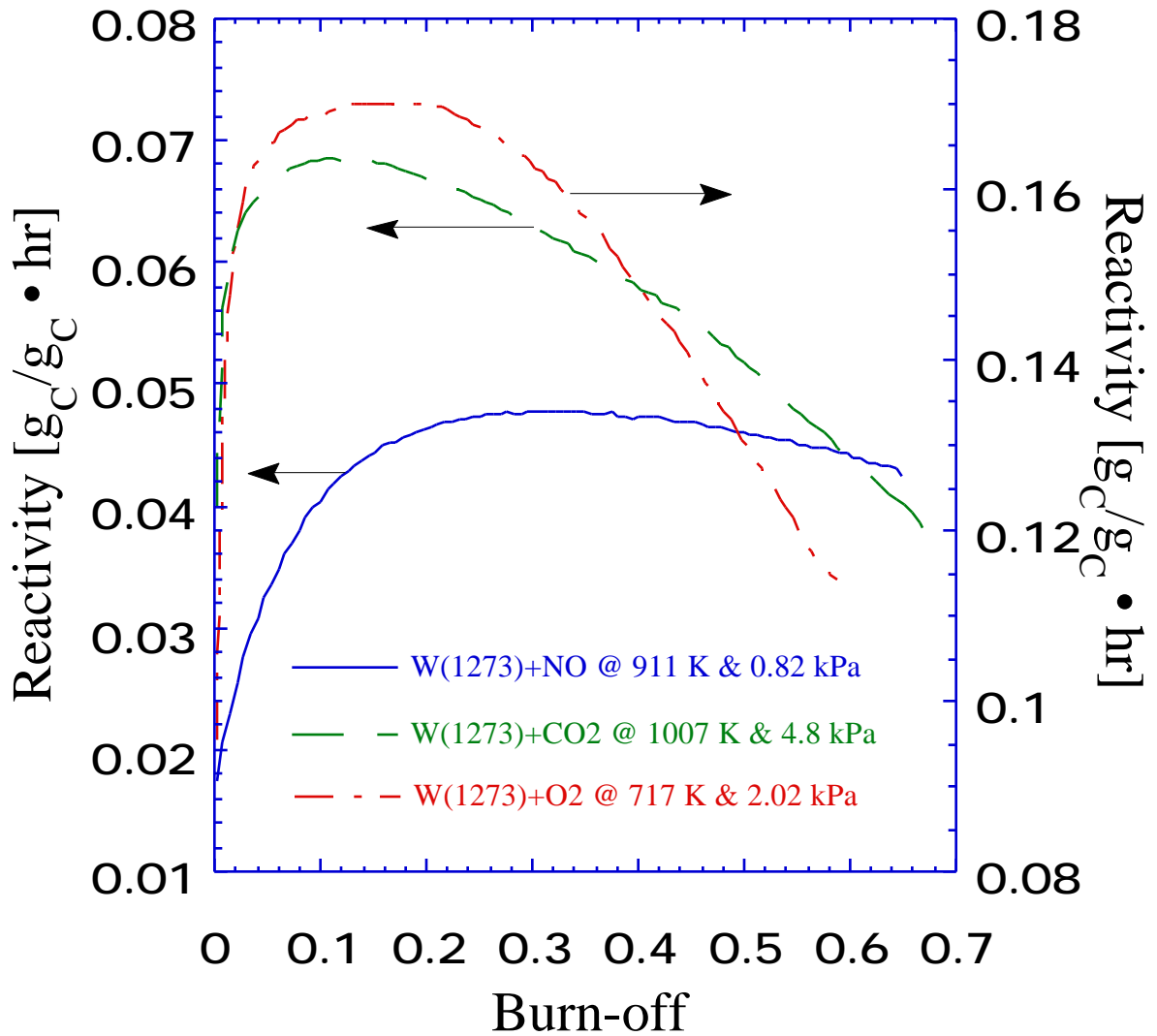


Figure 15. Reactivity vs. burn-off curves for Wyodak coal char in different oxidizing gases. Reactivity expressed as $\frac{1}{m_0} \frac{dm}{dt}$.

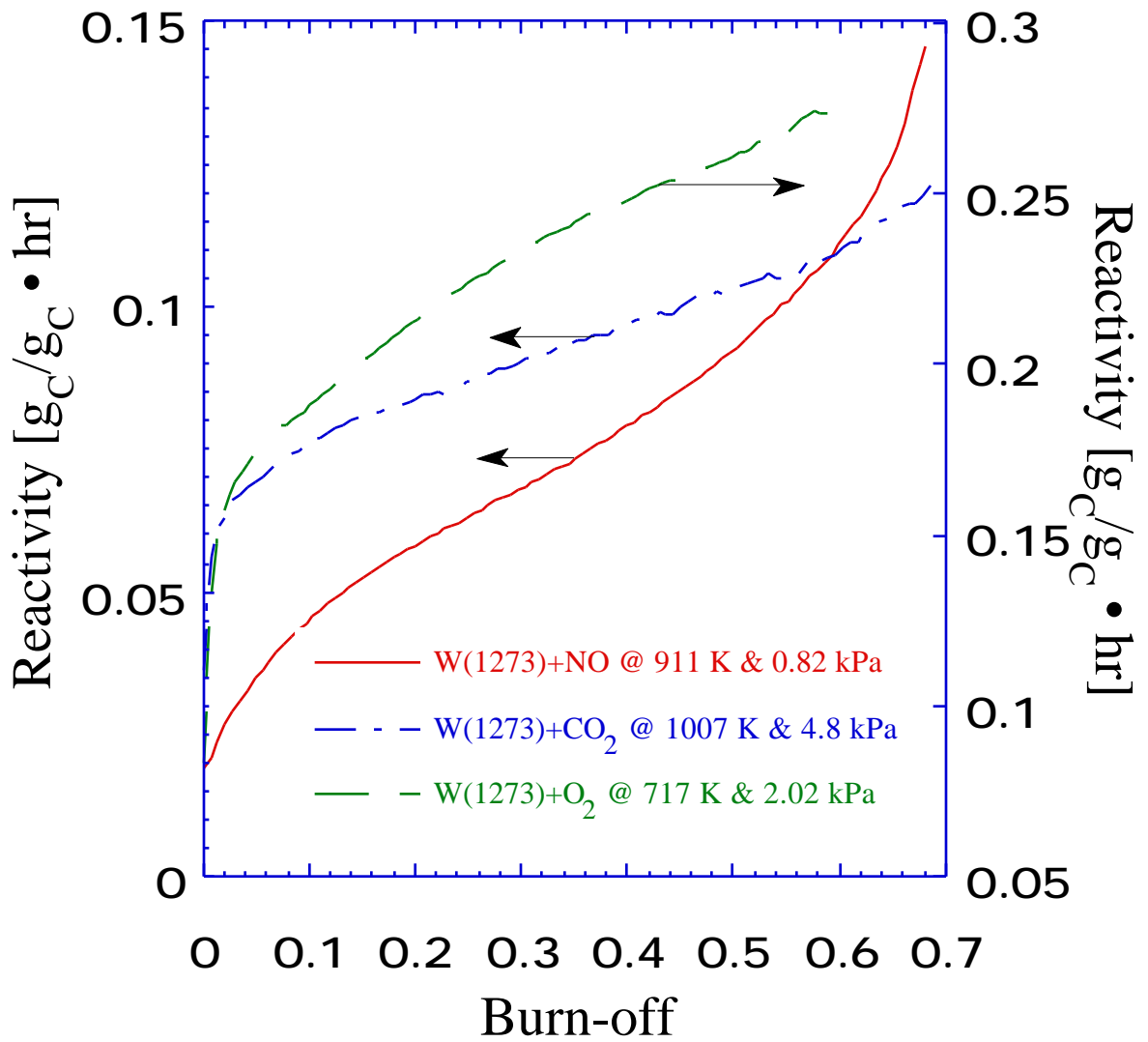


Figure 16. Reactivity vs. burn-off curves for Wyodak coal char in different oxidizing gases. Reactivity expressed as $\frac{1}{m} \frac{dm}{dt}$.

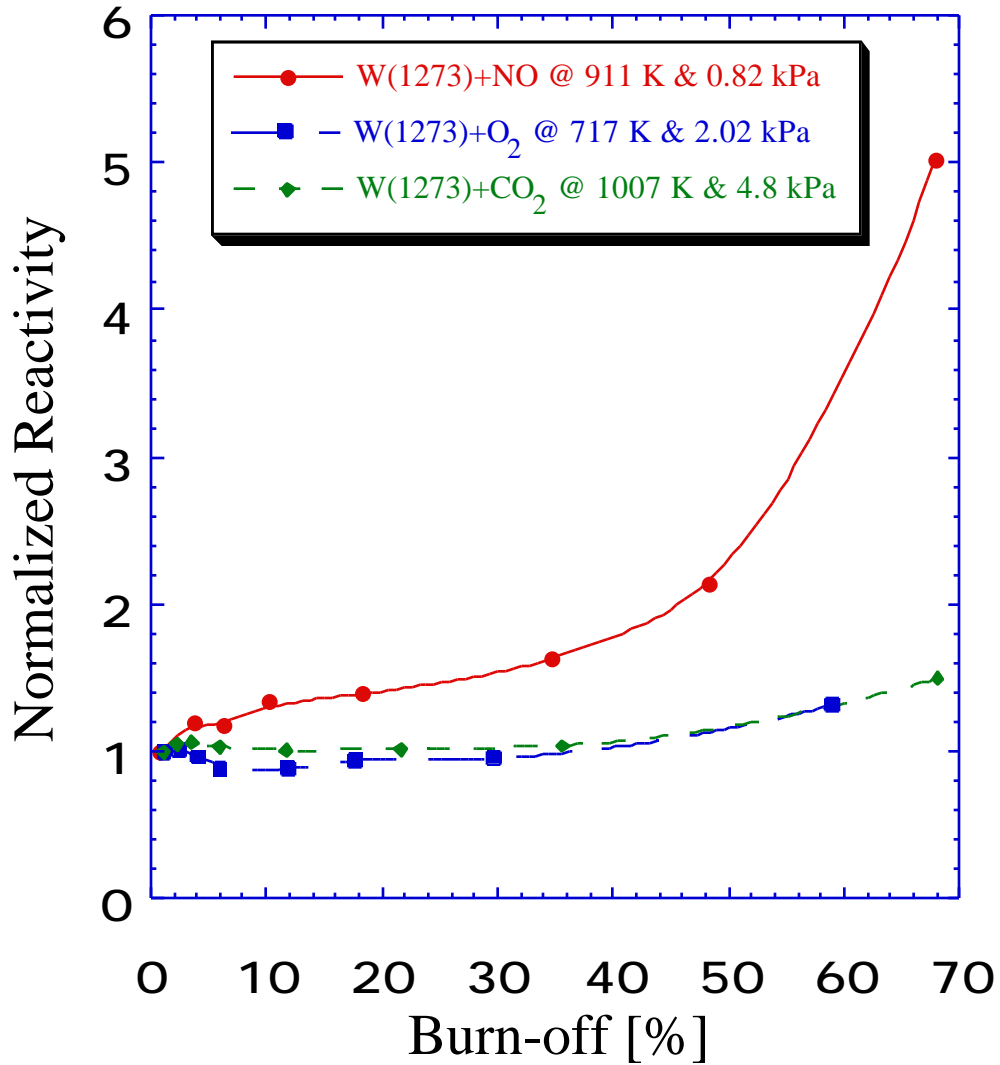


Figure 17. Reactivity vs. burn-off curves for Wyodak coal char in different oxidizing gases. Reactivity per unit N₂ BET surface area expressed as $\frac{1}{A} \frac{dm}{dt}$, and normalized with the reactivity at 1% burn-off.

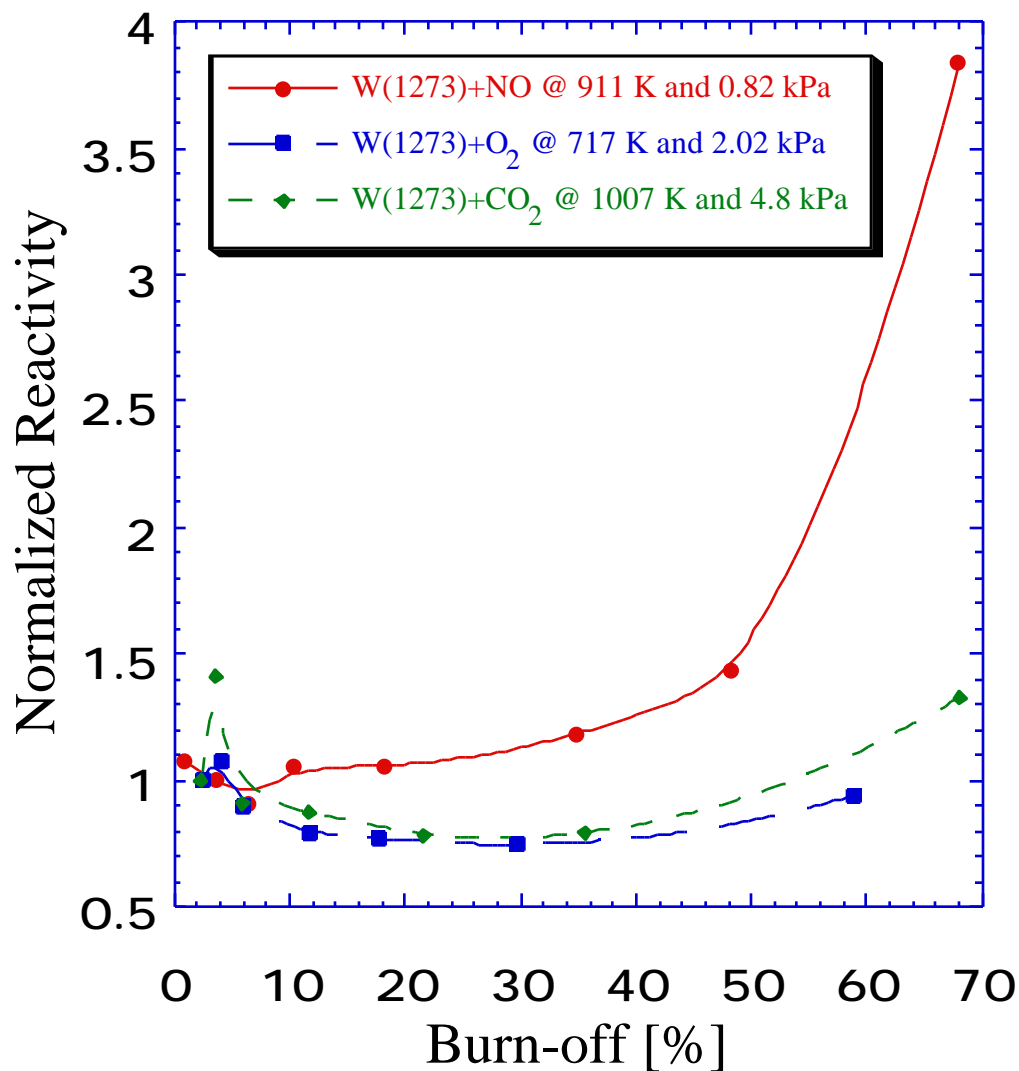


Figure 18. Reactivity vs. burn-off curves for Wyodak coal char in different oxidizing gases. Reactivity per unit Ar BET surface area expressed as $\frac{1}{A} \frac{dm}{dt}$, and normalized with the reactivity at 1% burn-off.

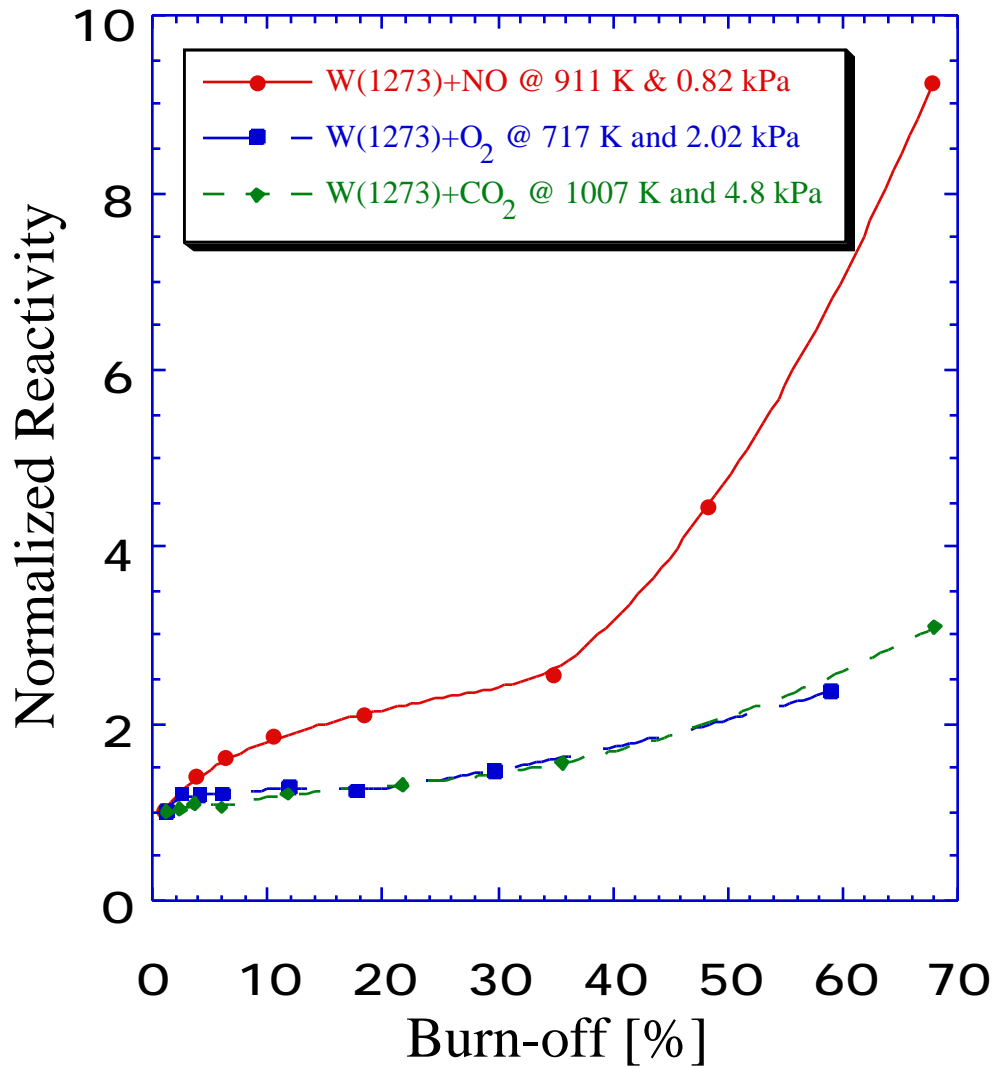


Figure 19. Reactivity vs. burn-off curves for Wyodak coal char in different oxidizing gases. Reactivity per unit CO₂ BET surface area expressed as $\frac{1}{A} \frac{dm}{dt}$, and normalized with the reactivity at 1% burn-off.

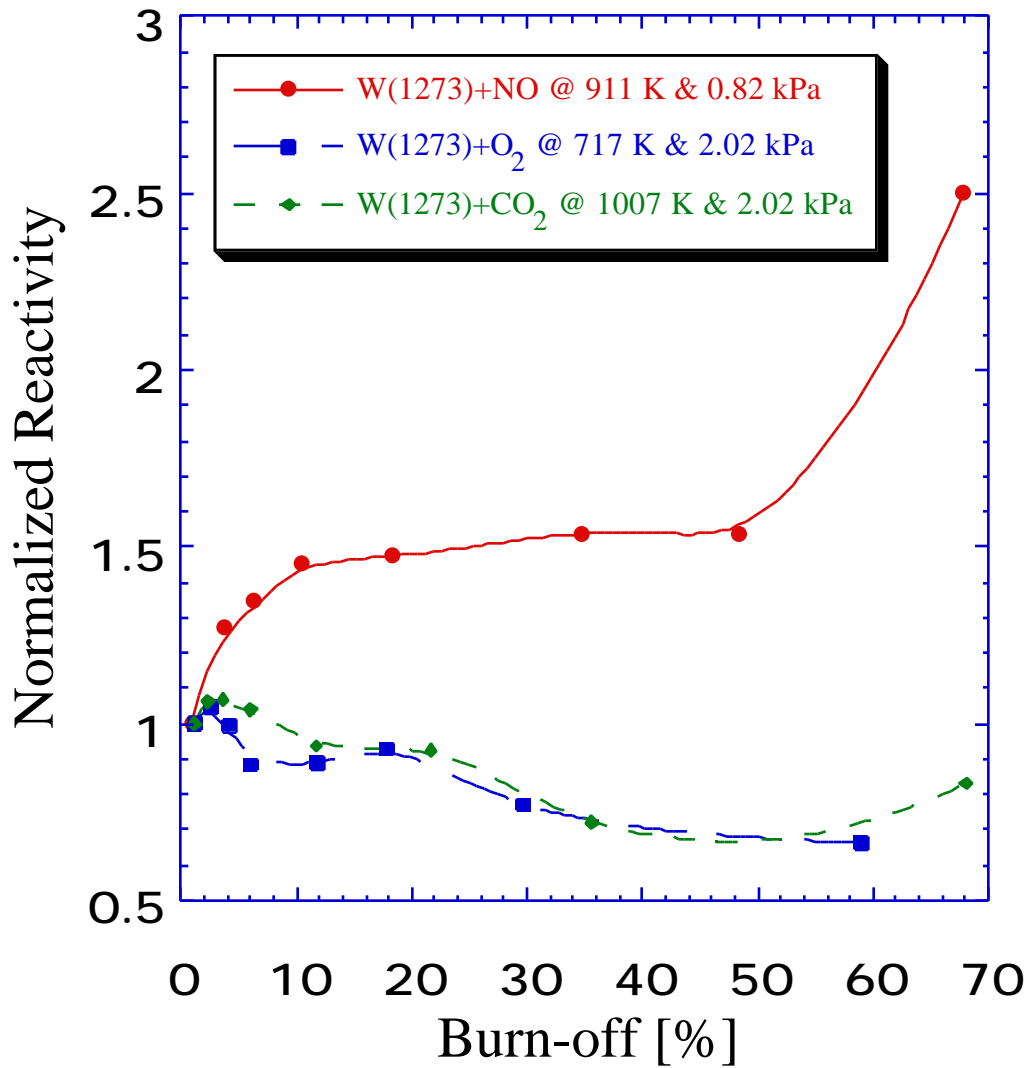


Figure 20. Reactivity vs. burn-off curves for Wyodak coal char in different oxidizing gases. Reactivity per unit N₂ total volume expressed as $\frac{1}{V} \frac{dm}{dt}$, and normalized with the reactivity at 1% burn-off.

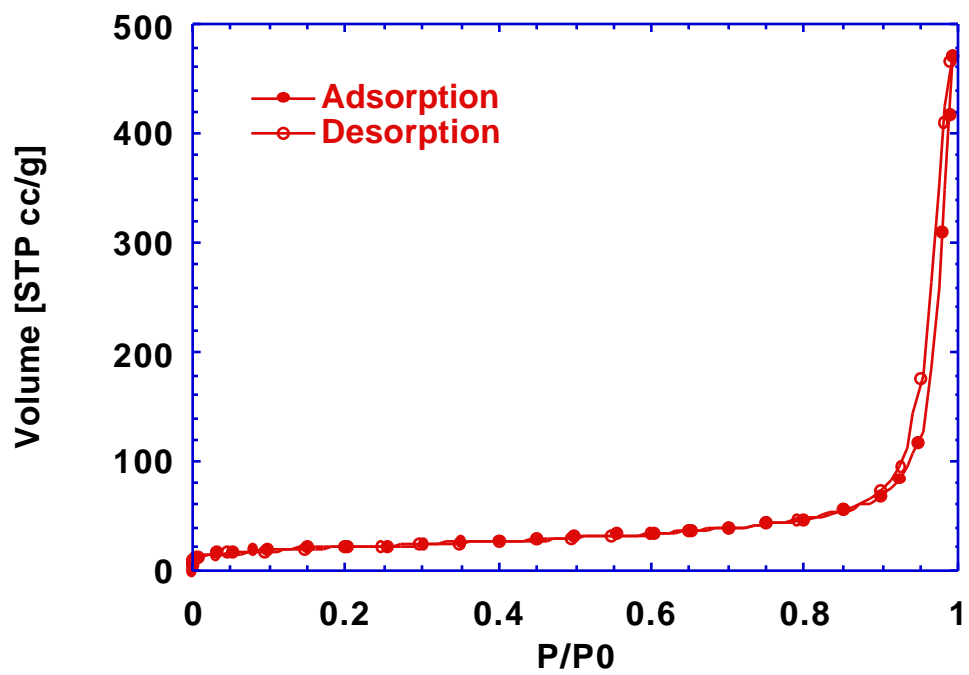


Figure 21. Nitrogen isotherms for raw tire char.

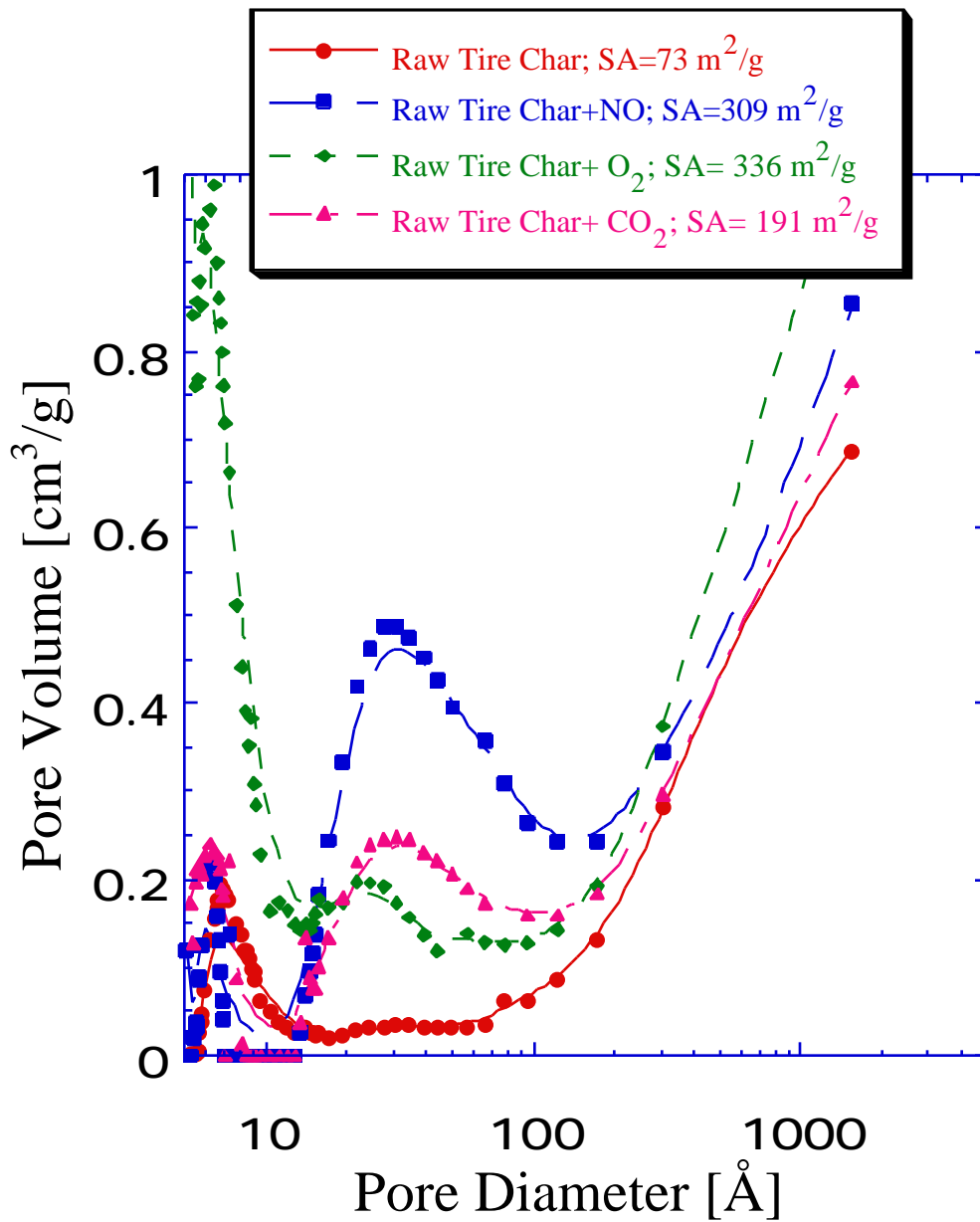


Figure 22. BJH pore size distributions of raw tire chars before and after gasification in different atmospheres. Data from adsorption branch of N₂ isotherm.

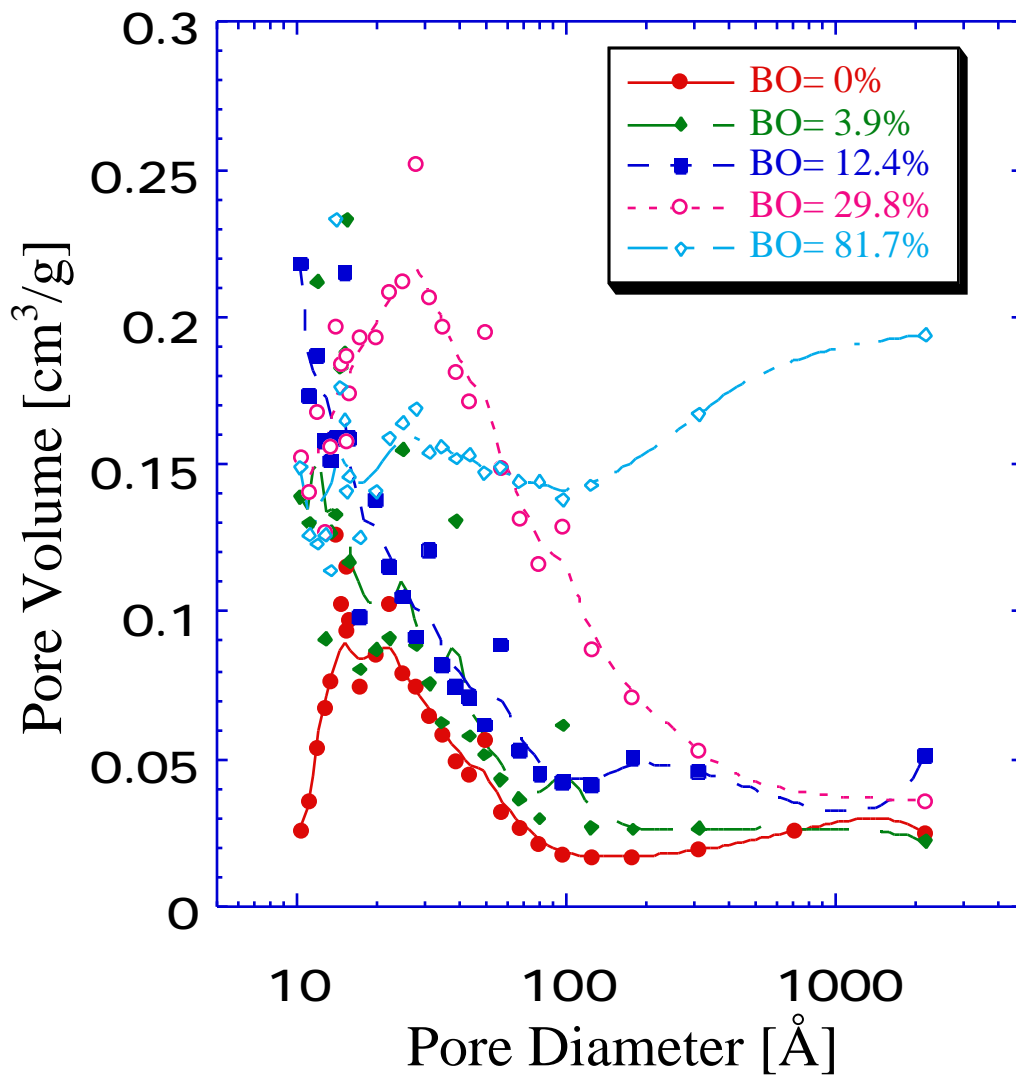


Figure 23. Pore size distribution for Wyodak coal char determined at different levels of burn-off in NO (Zone II). Samples were prepared in 0.82 kPa of NO at 1027 K. Data from adsorption branch of N₂ isotherm.

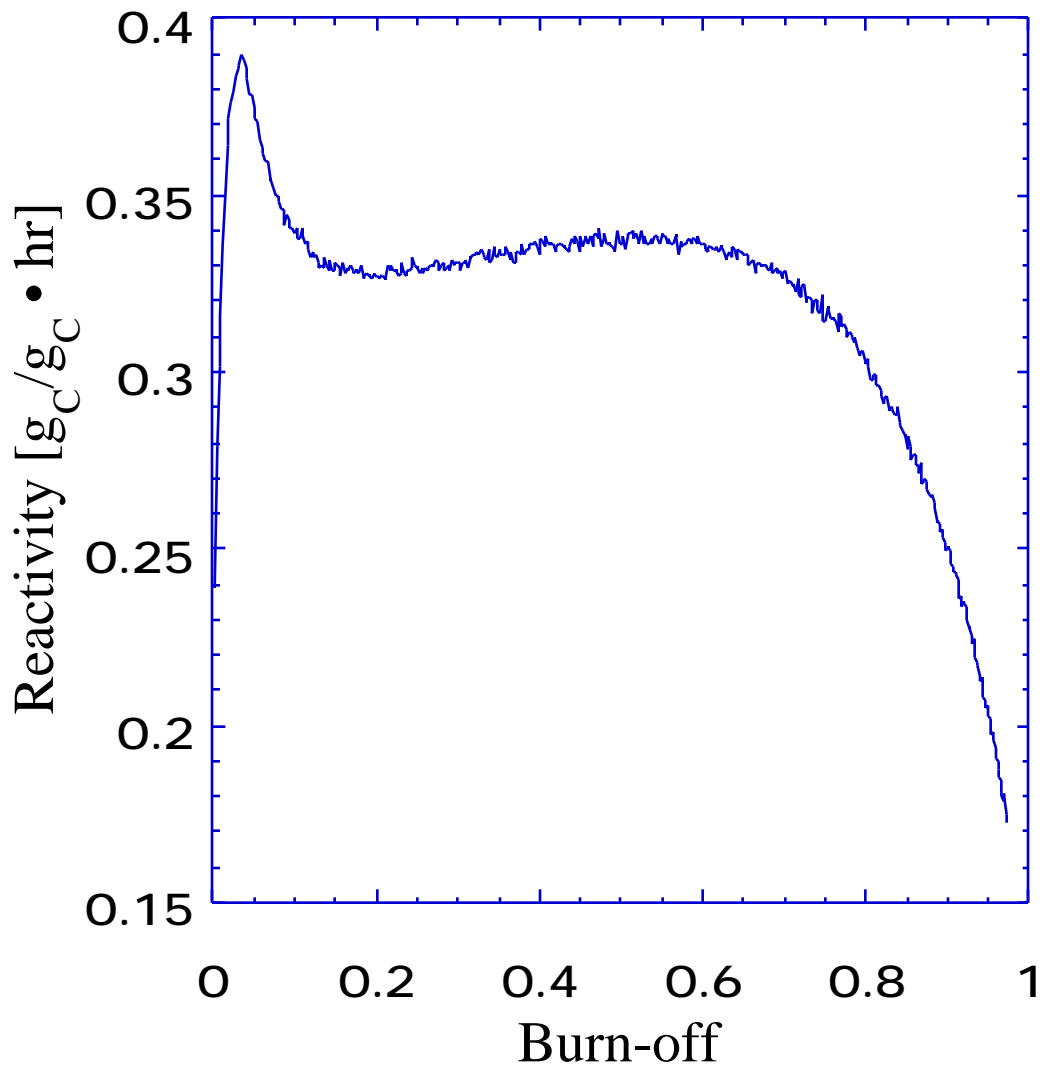


Figure 24. Reactivity vs. burn-off curves for Wyodak coal char in NO at 1027 K (Zone II). Reactivity is expressed as $\frac{1}{m_0} \frac{dm}{dt}$

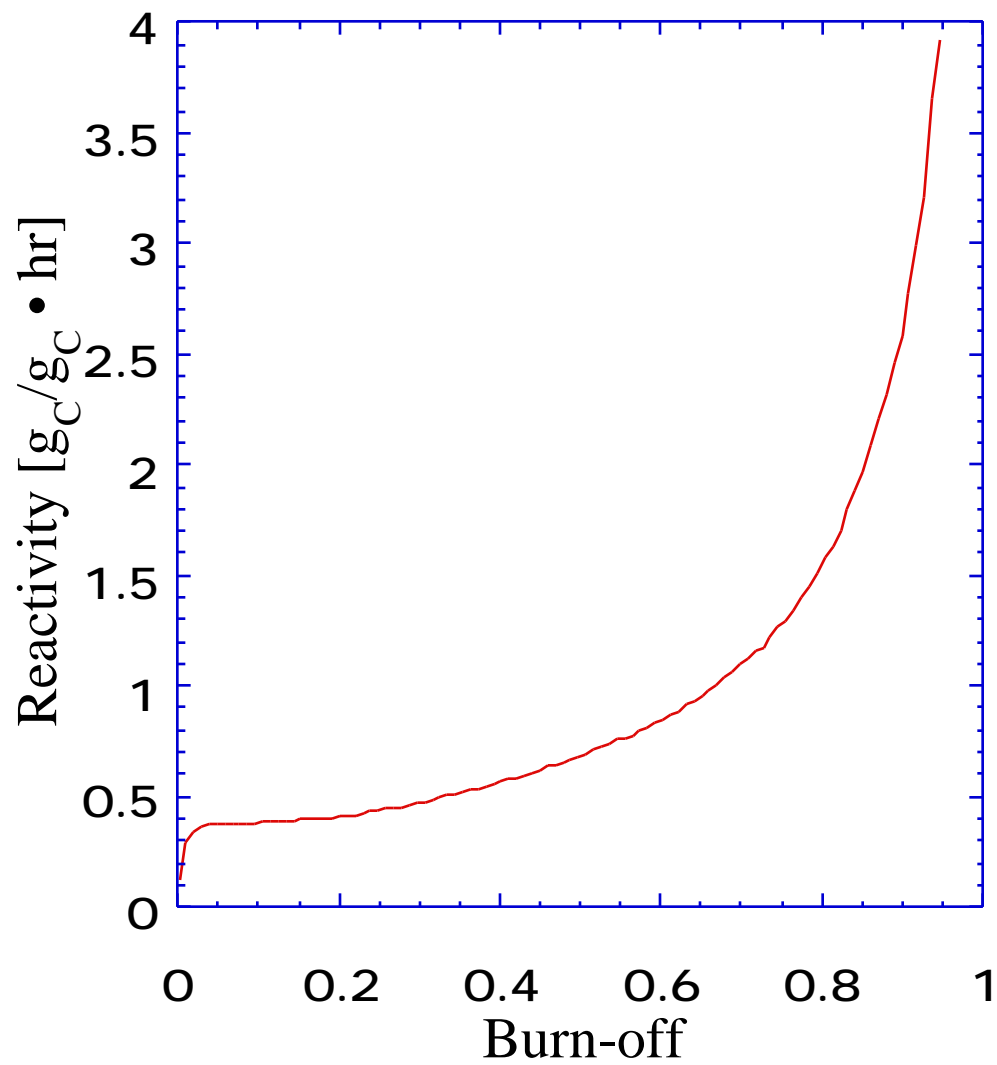


Figure 25. Reactivity vs. burn-off curves for Wyodak coal char in NO at 1027 K (Zone II). Reactivity is expressed as $\frac{1}{m} \frac{dm}{dt}$.

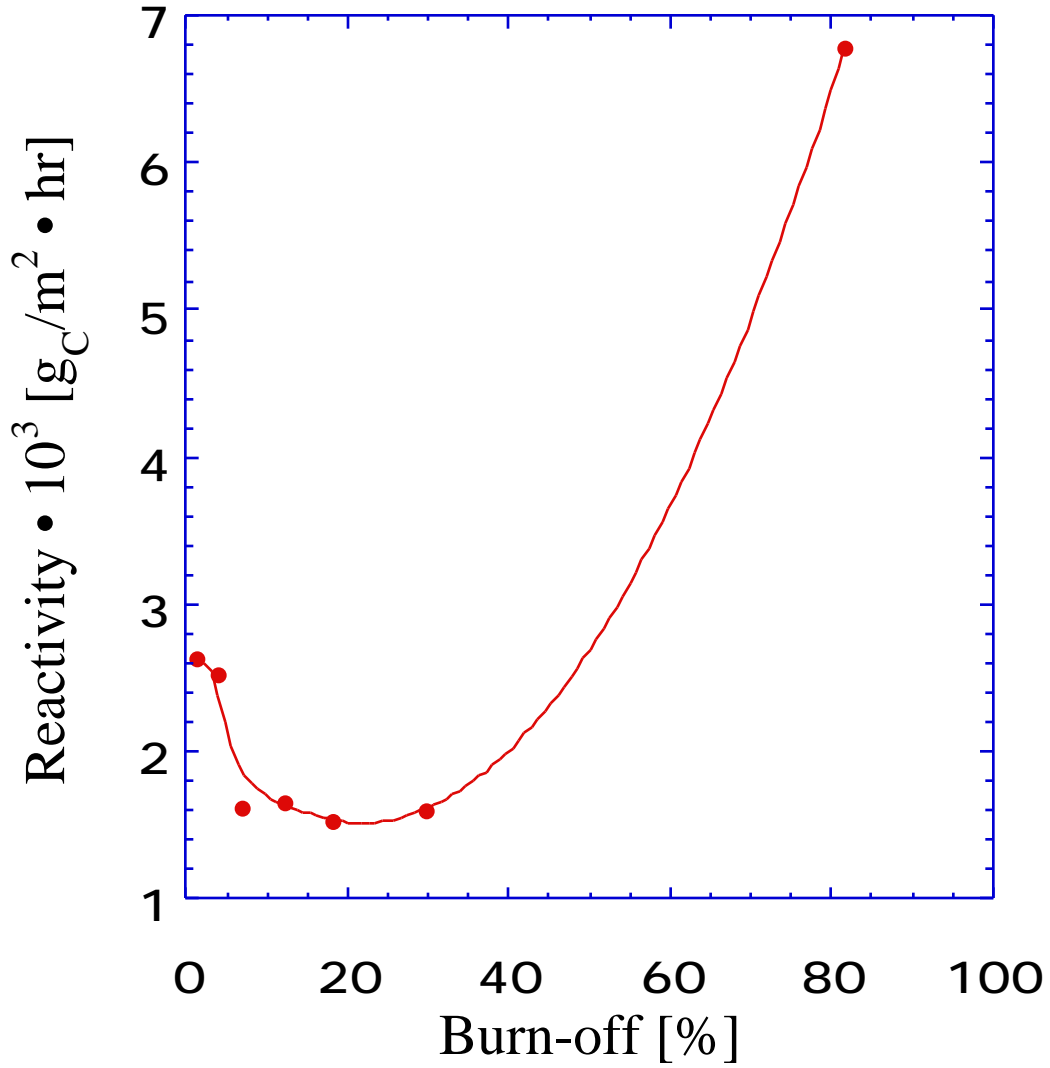


Figure 26. Reactivity vs. burn-off curves for Wyodak coal char in NO at 1027 K (Zone II). Reactivity is expressed as $\frac{1}{m} \frac{dm}{dt}$ and normalized with N₂ BET surface area.